UNIVERSITY OF CALIFORNIA, SAN DIEGO

Single Molecule Studies of Genome Packaging in Bacteriophage Phi29 Reveal Nonequilibrium DNA Dynamics and Continuous Allosteric Regulation of the Packaging Motor Complex

A dissertation submitted in partial satisfaction of the

requirements for the degree of Doctor of Philosophy

in

Chemistry

by

Zachary T. Berndsen

Committee in charge:

Professor Douglas E. Smith, Chair
Professor Kamil Godula
Professor Alex Groisman
Professor Patricia Jennings
Professor Elizabeth Komives

2015

The dissertation of Zachary T. Berndsen is approved, and it is acceptable in quality and form for publication on microfilm:

_____

_____

_____

_____

_____

Chair

University of California, San Diego

2015

DEDICATION

I dedicate this work to my family in recognition of their unconditional support.

TABLE OF CONTENTS

Signature Page ……iii

Dedication ……iv

Table of Contents v

Lists of Figures and Tables ix

Acknowledgements x

Vita xii

Abstract of the Dissertation ..…….....xiii

Chapter I **Introduction** ...…….....1

A. Bacteriophage phi29 as a model system 2

B. Genome packaging in bacteriophage 3

C. The bacteriophage DNA packaging motor 4

D. The state of the field ....…….....….5

E. References ...…….....….8

Chapter II **Nonequilibrium dynamics and ultraslow relaxation of confined DNA during viral packaging** …….....10

A. Introduction 11

B. Materials and methods ..…….....12

1. Biochemical Reagents 13

2. Optical Tweezers 13

3. Single-molecule packaging assay 14

4. Data analysis 14

C. Results 15

1. Acceleration of DNA packaging after long stalls 15

2. Heterogeneous dynamics 18

3. Packaging with spermidine3^{+} dramatically increases heterogeneity in packaging rates 20

4. The duration and frequency of intrinsic motor pausing is reduced after long stalls 21

D. Discussion 23

1. The packaged DNA adopts a non-equilibrium structure at high filling 23

2. Comparison with theoretical studies of DNA packaging 24

3. Comparison with structural data 24

4. Comparison to studies of polymer dynamics under tight Confinement 25

5. Conclusions 27

E. References 28

Chapter III Continuous Allosteric Regulation of the Phi29 Packaging Motor by a Sensor that Detects the Density and Conformation of the Packaged DNA 33

A. Introduction 34

B. Materials and methods 36

1. Biochemical Reagents 36

2. Optical Tweezers 37

3. Single-molecule packaging assay and nucleotide exchange experiments 38

4. Data analysis 38

5. Simulations of the phi29 DNA packaging motor 39

i. The mechanochemical model 39

ii. Monte Carlo simulations 41

iii. Setting the rate constants at low filling 44

C. Results 50

1. Motor restart time after γS-ATP induced stalls increases sharply with procapsid filling 50

2. The frequency and duration of intrinsic motor pausing increases with filling but not with force 53

3. The frequency of motor slipping increase with applied load but not with filling 56

D. Discussion 57

1. An unconventional type of allosteric regulation 57

2. Structural basis for allosteric affect 59

3. Distinction between the effects of load and allosteric regulation 62

4. Effect on motor ATP interactions 62

5. Contributions of load vs. allosteric regulation to motor slowing 63

6. Forces resisting DNA confinement and comparisons with theories.....66

7. Regulation responds to changes in both length and conformation of packaged DNA 67

8. Relationship with motor stepping kinetics 69

9. Monte Carlo simulations 70

10. Conclusions 73

E. References 75

Chapter IV Final Thoughts and Future Directions 80

A. Future Directions 81

1. Achieving long timescale aging experiments with DNA ejection 83

B. Concluding Remarks 90

C. References 96

LIST OF FIGURES AND TABLES

Figure 2.1. Motor stall-restart experiments ……..……...….16

Figure 2.2. Heterogeneity in packaging dynamics ……..…...…….…..19

Figure 2.3. Motor pausing ……...……..……..…....22

Figure 3.1. Components of the phi29 packaging complex ……..……...…….35

Table 3.1. Simulation parameters.....47

Figure 3.2. Simulation results at low filling and low force…….....48

Figure 3.3. Nucleotide exchange experiments ……....……..…….51

Figure 3.4. Analysis of pauses in motor translocation ……..……....54

Figure 3.5. Analysis of motor slipping …….....55

Figure 3.6. Motor velocity measurements ……..……..58

Figure 3.7. Two different mechanisms of regulation of the phi29 motor ……..……..61

Figure 3.8. Factors influencing reduction in motor velocity 64

Figure 3.9. Monte Carlo simulations of allosteric motor regulation …….…….…….71

Figure 4.1. Flow chart illustrating our understanding of the underlying biophysical phenomena involved in DNA packaging ...….....…….…….82

Figure 4.2. Osmotic suppression of ejection …….…….....…..86

Figure 4.3. DNA ejection after 24hr aging …….....88

ACKNOWLEDGEMENTS

I would like to acknowledge those people who have contributed in a significant way to the work presented in this dissertation as well as those of who have provided personal support to me throughout this process. First and foremost, I must thank my family. My parent's and my brother's healthy mix of conditional and unconditional support has always been a foundation for my success and the past five years have been no exception. I would also like to acknowledge my brother for his support in scientific and technical matters, particularly those pertaining to computer science and signal processing for which I had little formal training.

My advisor, Doug Smith, above all else, has helped to develop in me the mind of a scientist. He was always available to provide guidance and enlightening discussion when I needed it and his expertise is unmatched. He understood my strengths and weaknesses as a biochemist in an experimental physics lab and was patient and encouraging towards my desires to pursue some of the more complicated physics problems. The countless hours he spent with me preparing manuscripts for publication were invaluable in my development as a clear and effective scientific communicator. He taught me a lot about how to think through difficult problems and how to design practical and efficient scientific experiments. Most importantly, he is a true skeptic and never one to take himself too seriously, which should be traits of any good scientist

I would also like to thank our terrific collaborators, Shelly Grimes and Paul Jardine, at the University of Minnesota who were responsible for the production of all the viral components used in this research and without whom we could not do what we do. They are expert biochemists and their advice and guidance was invaluable throughout my

time working with phi29. They were always ready to help when we needed more reagents or tips on how to overcome challenges with the packaging assay.

Finally, I want to thank my fellow lab workers. First, Amy Davenport for her initial support during my rotation through the lab and helping me decide to join as a permanent member. I would like to thank Damian DelToro for helping train me on the optical tweezers and in flow cell construction. I wish to thank Mariam Ordyan for her support in creating modified DNA constructs. I would like to thank Nick Keller for his invaluable efforts towards the construction and maintenance of the optical tweezer system used in all the experiments presented here as well as for his efforts as my primary collaborator on the two main projects presented in this work.

Chapter II, in full, is a reprint that the dissertation author was the principal researcher and author of. The material appears in *PNAS*. (**Z. T. Berndsen,** N. Keller, S. Grimes, P. J. Jardine, D. E. Smith. (2014). Nonequilibrium dynamics and ultraslow relaxation of confined DNA during viral packaging, *Proceedings of the National Academy of Science,* 111, 8345)

All of Chapter III except sections **B.5** and **D.8**, and Figs. 3.2 and 3.8, and table 3.1, is a reprint that the dissertation author was the principal researcher and author of. The material appears in *Biophysical Journal*. (**Z. T. Berndsen,** N. Keller, D. E. Smith. (2015). Continuous Allosteric Regulation of a Viral Packaging Motor by a Sensor that Detects the Density and Conformation of Packaged DNA, *Biophysical Journal*, 108 (2), 315-324)

VITA

2010 Bachelors of Art, Biochemistry, DePauw University, Greencastle, IN

2012 Masters of Science, Chemistry, University of California, San Diego

2015 Doctor of Philosophy, Chemistry, University of California, San Diego

PUBLICATIONS

Z. T. Berndsen, N. Keller, S. Grimes, P. J. Jardine, D. E. Smith (2014) Nonequilibrium dynamics and ultraslow relaxation of confined DNA during viral packaging. Proceedings of the National Academy of Sciences USA 111, 8345

Z. T. Berndsen, N. Keller, D. E. Smith (2015) Continuous Allosteric Regulation of a Viral Packaging Motor by a Sensor that Detects the Density and Conformation of Packaged DNA. Biophysical Journal 108 (2), 315-324

FIELDS OF STUDY

Major Field: Molecular Biophysics

Studies in Molecular Biology and Biological Physics

Professor Douglas E. Smith

HONORS AND AWARDS

2011-2013 Molecular Biophysics Training Grant Recipient

ABSTRACT OF THE DISSERTATION

Single Molecule Studies of Genome Packaging in Bacteriophage Phi29 Reveal Nonequilibrium DNA Dynamics and Continuous Allosteric Regulation of the Packaging Motor Complex

by

Zachary T. Berndsen

Doctor of Philosophy in Chemistry

University of California, San Diego, 2015

Professor Douglas E. Smith, Chair

The high-density packaging of DNA in many viruses is a process that requires the action of powerful molecular motor complexes that couple the energy of ATP hydrolysis to the movement of DNA into the viral prohead. Besides being a key step in viral assembly, DNA packaging is a general model for understanding the physics of tightly confined polymers. A fundamental question raised in the literature is whether packaging can be modeled as a quasistatic thermodynamic process, in which the DNA relaxes

quickly to equilibrium, or whether it involves nonequilibrium dynamics. The nature of the DNA dynamics at high prohead fillings and its relationship to the precise mechanochemical cycle of the packaging motor remain an open question. This work is aimed at investigating that relationship via single molecule optical tweezers experiments.

In Chapter II I report the results of experiments in which we directly measure the packaging of single DNA molecules in bacteriophage phi29 with optical tweezers. Using a new technique in which we stall the motor and restart it after increasing waiting periods, we show that the DNA undergoes nonequilibrium conformational dynamics during packaging. We show that the relaxation time of the confined DNA is >10 min, which is longer than the time to package the viral genome and 60,000 times longer than that of the unconfined DNA in solution. Thus, the confined DNA molecule becomes kinetically constrained on the timescale of packaging, exhibiting glassy dynamics, which slows the motor, causes significant heterogeneity in packaging rates of individual viruses, and explains the frequent pausing observed in DNA translocation. These results support several recent hypotheses proposed based on polymer dynamics simulations and show that packaging cannot be fully understood by quasistatic thermodynamic models.

In Chapter III I report evidence for an unconventional type of allosteric regulation of a biomotor. We show that the genome-packaging motor of phage phi29 is regulated by a sensor that detects the density and conformation of the DNA packaged inside the viral prohead, and slows the motor by a mechanism distinct from the effect of a direct load force on the motor. Specifically, we show that motor-ATP interactions are regulated by a signal that is propagated allosterically from inside the viral shell to the motor mounted on the outside. This signal continuously regulates the motor speed and pausing in response

to changes in either density or conformation of the packaged DNA, and slows the motor before the buildup of large forces resisting DNA confinement. Analysis of motor slipping reveals that the force resisting packaging remains low (<1 pN) until ~70% and then rises sharply to ~23 pN at high filling, which is a several-fold lower value than was previously estimated under the assumption that force alone slows the motor. These findings are consistent with recent studies of the stepping kinetics of the motor. The allosteric regulatory mechanism we report allows double-stranded DNA viruses to achieve rapid, high-density packing of their genomes by limiting the buildup of nonequilibrium load forces on the motor.

In Chapter IV I attempt to synthesize the previous chapters into a more unified picture and reflect on what I learned and the implications of our findings. I also discuss a few of the numerous projects that can expand upon the work already completed here, focusing particularly on using DNA ejection measurements to study DNA relaxation on much longer timescale than would be possible with single molecule experiments.

Chapter I

Introduction

A. Bacteriophage phi29 as a model system

Bacteriophage research has been at the forefront of molecular biology since the very beginning, with many of the most fundamental breakthroughs in the field being made by scientists studying bacteriophage. Bacteriophage are to molecular biology what the hydrogen atom is to quantum mechanics, or the fruit fly to genetics. These systems didn't acquire such a foundational status within their fields by chance but because they all share the traits of a perfect model system. Such systems have to be complex enough to be relevant yet simple enough to be understood almost completely. Bacteriophage are the most numerous biological entities on the planet by far, and one of the oldest, representing an enormous amount of genetic diversity and possessing complex phylogenies. Genetic diversity means functional and structural diversity which has made bacteriophage an important model system for geneticists and structural biologist. Bacteriophages are bacterial viruses and thus walk the line between living and nonliving matter which makes them slightly less foreign to the curious physicist who probably doesn't like chemistry or squishy stuff, helping to bringing many talented physicists into the field of biology. So it should come as no surprise that bacteriophage research is still driving scientists to push boundaries in cutting edge fields.

If bacteriophage is the model system of molecular biology then phi29 is the model system of that model system. Other than phage lambda, phi29 is one of the most widely studied due to its relative size and simplicity, high particle yield per cell, and highly efficient in vitro assembly (1). Its 19.3kbp linear double-stranded genome only encodes 20 proteins, which is very small compared to other phages like T4 that encode hundreds.

This makes phi29 especially well suited as a model system for studying the biophysical processes involved in viral assembly which complement the comprehensive biochemical and genetic analysis. In the talented hands of our collaborators the yield and efficiency of the *in vitro* assembly assay are unparalleled in the field (2).

B. Genome packaging in bacteriophage

One of the most striking features of bacteriophage and what often captures the initial attention and imagination of young scientists is their physical appearance (usually captured by an electron microscope), and the most prominent feature of which is the fully packaged capsid. Usually in the shape of a 12-fold symmetric dodecahedron with and number of long spiderlike appendages protruding from it, it looks more like an alien space probe than anything that might be alive. However it's the DNA inside the capsid that is so important and exactly how it got inside that is such a mystery. At first people thought the capsid might assemble around the genome. However, to the astute scientist, a few simple calculations would quickly lead them away from such a hypothesis. For instance, using phage phi29 as an example which has a 19.3kbp genome and procapsid diameter of ~50 nm, we see that its genome is ~130x longer than the space in which it has to fit. Placed in perspective that is ~13ft of genome into a 1 inch capsid with the DNA diameter of scaling to ~1mm. In solution, the phi29 genome forms a loose random coil with a radius of gyration of ~500 nm and therefore must compact ~10,000x to fit inside the procapsid. Surely entropic penalties alone would prevent this from happening passively, not to mention bending and electrostatics. Because of its double helical shape, DNA is extremely stiff (3), not changing its direction significantly over ranges of ~ 50

nm, which here matches the diameter of the capsid, indicating the molecule must undergo significant bending stress upon compaction. DNA also has one of the highest linear charge densities of any polymer leading to large electrostatic penalties for such an extreme compaction. So, it should now seem clear that this process is not likely to occur passively and must involve a rather large input of energy.

C. The bacteriophage DNA packaging motor

Bacteriophage accomplish this remarkable feat with the aid of an intricate molecular motor complex positioned along with the portal protein at a unique 5-fold symmetric vertex at the base of the prohead (4). These motor proteins are members of the widely studied AAA+ superfamily of ATPases. These ATPases naturally form into homomeric ring oligomers often composed of 6 copies of themselves; however the phi29 ATPase forms a pentamer when bound to the procapsid (5). These ATPases complexes are involved in a wide variety of cellular activities and are known to operate through an intricate coordination of conformational changes associated with the different stages of the ATP hydrolysis cycles and coupled substrate interactions. The bacteriophage packaging ATPase utilizes a power-stroke mechanism whereby the free energy extracted from ATP hydrolysis is converted into mechanical movement along the DNA substrate. These motors are capable of remarkable energetic efficiency and catalytic turnover rates, with the T4 motor clocking in at over 1,000 bp packaged per sec (6). Early theoretical treatments of the DNA packaging phenomena predicted, as one would expect, that these motor must be very powerful; capable of overcoming the entropic, bending, electrostatic, and hydrodynamic forces associated with genome compaction estimated to reach as high

as 20 pN (for phage dimensions similar to phi29 (7)). Indeed, pioneering work by our lab revealed that the phi29 packaging motor can generate forces in excess of 60 pN (a value between old and new estimates), making it the most powerful molecular motor ever studied

D. The state of the field

Despite being at the center of the collective scientific conscious of an entire field for so long, new and interesting discoveries are still being made studying bacteriophage DNA packaging. Surprisingly (or not), interest in modeling the physics of DNA compaction has attracted a remarkable amount of attention from the theoretical and computational physics and engineering communities, with well over 100 highly diverse published modeling studies in the past 10 years alone. This trend can be seen as a direct consequence of the development by our lab of an *in vitro* single-molecule packaging assay where an optical tweezers system allows for the direct application and measurement of forces on the motor (8). These models range from analytical polymer physics and course grained simulation to physically packaging macroscopic wires into containers. The studies vary widely in their treatment of DNA, genome lengths considered, capsid size and shape modeled, treatment of ionic interactions, and equilibration procedure. Although such a body of work can be quite overwhelming for one person to attempt to make sense of, collective trends start to emerge leading to a kind of unofficial consensus and many new predictions are made that can be tested experimentally.

Being a member of one of maybe three labs studying the biophysics of the packaging process experimentally, this means we never have a shortage of new experiments to try, but it also means our data will be widely scrutinized and compared to theoretical predictions. This process lead to fairly significant discrepancies being identified between the forces predicted to resist the packaging motor and the ones we were measuring in our optical tweezers assay. Specifically, the forces we were calculating based on changes in the velocity implied that the force resisting packaging exceeded 100pN by the end of the reaction and began to build up almost immediately after packaging was initiated (9), whereas most theoretical treatment didn't predict any forces until near completion that usually maxed out around ~20 pN (7) (though these estimates do vary fairly significantly depending on the model). There are only three possible conclusions to draw from this; either experiments are right and the theories need revision, theories are right and the results of the experiments need to be reassess, or both groups are each a little wrong.

This was the state of the field when I joined the lab in 2011 and previous members had and already begun thinking about potential ways to root out the source of this discrepancy. Several factors were potential candidates. First, the DNA inside phi29 may not be arranged in a coaxial spool as was the consensus equilibrium model at the time, which would change the theoretical force calculations. Inaccuracies in the estimates of capsid size could lead to significant changes in the force since many models predicted very different forces for phages of different capsid sizes and shapes. Or perhaps subtle yet unforeseen effects from complex ionic screening interactions are responsible, given that the largest discrepancies existed in the forces we measured at high Mg^{2+}

concentrations. Although the coaxial spool is a widely accepted, significant deviations from this perfect spool have been observed in several Cryo-electron microscopy (Cryo-EM) studies (10) as well as in dynamic simulations (11). Another possible scenario not accounted for by equilibrium models but observed in several dynamic simulations are dissipative dynamics, or in other words the formation of nonequilibrium structures (12). Because most models assume the reaction occurs in quasistatic equilibrium (the DNA is always able to quickly relax to its free energy minimized structure), then if energy is dissipated by the DNA during packaging the measured work done would be higher than the gain in potential energy leading to lower force predictions. This would have consequences on the comparisons of measured ejection and packaging forces as well, since it is normally assumed that the energy put into the system during packaging is available to drive ejection across the membrane.

In Chapter II I describe results from experiments designed specifically at testing the validity of this quasistatic assumption. Indeed, we find evidence for significant nonequilibrium dynamics and ultra-slow relaxation behavior of the packaged DNA at high filling that slow the motor, cause heterogeneity in packaging dynamcis, and cause frequent pausing of the motor. The effect these nonequilibrium dynamics have on the measured force resisting packaging however were not great enough to fully account for the differences between measured and predicted forces, especially at very low fillings were nonequilibrium effects were not observed but significant force was still measured, so it was clear there must be other unforeseen factors at play. In fact, it was an anomalous behavior observed while conducting these experiments that ultimately lead us to discover the real source of the discrepancies, and it was surprising and unexpected.

In Chapter III I describe this surprising discovery and our attempts to make sense of it. What we found is that in fact both the theory AND our interpretation of the experimental data were incorrect. Just as the equilibrium theories relied on the quasistatic assumption, we too relied on an unvalidated assumption. This assumption was that the observed slowing of the motor with procapsid filling was entirely due to forces which directly load the motor and was critical in converting velocities measured during packaging to forces via the well characterized force-velocity relationship of the motor. In other words, we assumed that the changes in velocity we observed when we apply a load to the motor in the direction opposite packaging with our optical tweezers we were slowing the same steps in the mechanochemical cycle of the motor that slow down with filling. This assumption was well justified considering what was known about other molecular motors and other DNA packaging motors at the time, however as you will read in Chapter III, is actually the primary reason why our estimates of force as well as the shape of the force vs filling relationship were so different than theoretically predicted.

In Chapter IV I summarize these two sets of data and discuss how they complement eachother to help us create a much clearer, albeit much more complicated, picture of the dynamic relationship between the nonequilibrium nature of the packaging process and the precise mechanochemical functioning of the motor. I discuss ways in which we can build off of these two discoveries and expand our understanding of them with new experiments and experimental techniques. I also present preliminary data from one such set of experiments that I find the most promising for continuing to study the nonequilibrium effects in particular.

E. References

1. Grimes S., Jardine P.J., Anderson D. (2005) Bacteriophage phi29 DNA Packaging. Advances in Virus Research, Vol. 58. Elsevier Science (USA).

2. Guo P., Grimes S. & Anderson, D. (1986) A defined system for in vitro packaging of DNA-gp3 of the Bacillus subtilis bacteriophage phi29. Proc. Natl Acad. Sci. USA 83, 3505–3509.

3. Wang, M. D., H. Yin, R. Landick, J. Gelles, and S. M. Block. (1997) Stretching DNA with optical tweezers. Biophys. J. 72:1335–1346.

4. Simpson A. A., Tao Y., Leiman P.G., Badasso M.O., He Y., Jardine P.J., Olson N.H., Morais M.C., Grimes S., Anderson D.L., Baker T.S., Rossmann M.G. (2000) Structure of the bacteriophage phi29 DNA packaging motor. Nature 408, 745–750.

5. M. Morais, J. Koti, V. Bowman, E. Reyes-Aldrete, D. Anderson, M. Rossmann (2008) Defining molecular and domain boundaries in the bacteriophage phi29 DNA packaging motor.Structure, 16, pp. 1267–1274.

6. Fuller D.N., Raymer D.M., Kottadiel V.I., Rao V.B., Smith D.E. (2007) Single phage T4 DNA packaging motors exhibit large force generation, high velocity, and dynamic variability. Proc. Natl. Acad. Sci. USA 104:16868–73

7. Tzlil S., Kindt J.T., Gelbart W.M. & Ben-Shaul A. (2003) Forces and pressures in DNA packaging and release from viral capsids. Biophys J 84(3): 1616-1627.

8. Smith D.E., Tans S.J., Smith S.B., Grimes S., Anderson D. L. & Bustamante C. (2001) The bacteriophage phi29 portal motor can package DNA against a large internal force. Nature 413(6857): 748-752.

9. Rickgauer, J. P., Fuller D.N., Grimes S., Jardine P.J., Anderson D., Smith D. E. (2008) Portal motor velocity and internal force resisting viral DNA packaging in bacteriophage phi29. Biophys. J. 94:159-167.

10. Comolli L.R., Spakowitz A.J., Siegerist C.E., Jardine P.J., Grimes S., Anderson D.L., Bustamante C., Downing K.H. (2008) Three-dimensional architecture of the bacteriophage phi29 packaged genome and elucidation of its packaging process. Virology 371(2): 267-277.

11. Ali I, Marenduzzo D & Yeomans JM (2004) Dynamics of polymer packaging. J Chem Phys 121(17): 8635-8641.

12. Forrey C & Muthukumar M (2006) Langevin dynamics simulations of genome packing in bacteriophage. Biophys J 91(1): 25-41.

Chapter II

Nonequilibrium dynamics and ultraslow relaxation of confined DNA during viral packaging

A. Introduction

DNA packaging is both a critical step in viral assembly and a unique model for understanding the physics of polymers under strong confinement. Before packaging, the DNA (~6–60 μm long) forms a loose random coil of diameter ~1–3 μm. After translocation into the viral prohead (~50–100 nm in diameter), a ~10,000-fold volume compaction is achieved. Packaging is driven by a powerful molecular motor that must work against the large forces resisting confinement arising from DNA bending, repulsion between DNA segments, and entropy loss (1–8).

DNA packaging in bacteriophages phi29, lambda, and T4 has been directly measured via single-molecule manipulation with optical tweezers and the packaging motors have been shown to generate forces of >60 pN, among the highest known for biomotors, while translocating DNA at rates ranging from ~100 bp (for phage phi29, which packages a 19.3-kbp genome into a 42 × 54-nm prohead shell) up to as high as ~2,000 bp/s (for phage T4, which packages a 171-kbp genome into a 120 × 86-nm prohead) (9–15). The force resisting packaging rises steeply with prohead filling and has been proposed to play an important role in driving viral DNA ejection (16).

Recently, a variety of theoretical models for viral DNA packaging have been proposed (3–5, 17–21). The simplest treat DNA as an elastic rod with repulsive self-interactions and assume that packaging is a quasistatic thermodynamic process, i.e., that the DNA is able to continuously relax to a free-energy minimum state (3–5, 19–21). The DNA arrangement is generally assumed to be an inverse spool with local hexagonal close packing between DNA segments, as suggested by electron microscopy and X-ray

scattering studies (22, 23). Such models yield exact analytical predictions that reproduce many of the experimental trends, including the sharp rise in resistance during the latter stages of packaging (3–5, 20).

Dynamic simulations, however, predict differing results. Depending on model and simulation protocol, some predict rapid equilibration into ordered spool or folded toroid conformations, whereas others predict nonequilibrium dynamics and disordered conformations (3, 6,–31). The packaged DNA conformation also depends on ionic conditions, prohead size and shape, and shape of the internal core structure found in some phages (6, 30). Notably, some electron microscopy studies have also been interpreted as suggesting ordered spooled conformations (22), whereas others have been interpreted as suggesting partly disordered conformations (29). Although some simulations predict nonequilibrium dynamics, several potential caveats are that (i) the DNA has been represented by coarse-grained polymer models with various approximations for physical interactions (6), (ii) the packaging rate used in the simulations is >105 times higher than the measured packaging rate due to computational constraints (3, 26–28), and (iii) it has been pointed out by some authors that simulation timescale cannot be directly related to experimental timescale because of the use of coarse-grained models for DNA (25, 28). As noted in early modeling studies, the calculations based on quasistatic models may represent a lower bound on the required packaging forces due to dissipative dynamic losses (4). Whether nonequilibrium dynamics play a significant role in real systems has thus remained an important open question.

B. Materials and Methods

1. Biochemical Reagents

For bacteriophage phi29 packaging components, fiberless proheads were produced by infection of *B. subtilis* 12A (*sup*-) with the ø29 mutant *sus* 8.5(900)-16(300)-14(1241) (defective in head fibers and the packaging ATPase) and purified as described previously (1). The packaging ATPase was produced from the plasmid pSACB-gp16 in *B. subtilis* and purified by chromatography as described previously (1), or produced as a fusion protein in the SUMO Pro vector (LifeSensors, Inc, Malvern, PA) and expressed in *E. coli* (2). The SUMO tag was subsequently cleaved off and removed by IMAC, yielding non-tagged ATPase. A 25 kbp dsDNA packaging substrate labeled at one end with biotin was prepared by PCR, as described previously (3), from a stock solution of lambda phage DNA using primers biotin-CTGATGAGTTCGTGTCCGTACAACTGGCGTAATC and aminoC_6-digoxigenin-ATCCGATCTGCGTTACCGAATGGATGGATG (Operon Inc.). This DNA was tethered to 2.8 μm diameter streptavidin coated microspheres as described previously (4, 5). Proprohead-motor complexes were pre-assembled and attached via anti-phi29 antibodies to 2.1 μm protein G coated microspheres as described previously (4, 5).

2. Optical Tweezers

Measurements were made with a dual-trap optical tweezers system as described previously (4, 5) and calibrated as described previously (6). Briefly, The dual-trap optical tweezers consists of a solid-state Nd:YAG laser (CrystaLaser, Reno, NV) split into two orthogonally polarized beams and focused by a water-immersion microscope objective (1.2 NA). One beam was steered by use of an acousto-optic deflector. The exiting beams

were collected by an identical objective, and the deflections of the fixed beam were measured by imaging the back focal plane of the objective onto a position-sensing detector . The custom three chamber flow cell is placed between the opposing objective so that the focal points of the traps are aligned with the central chamber of the flow cell.

3. Single Molecule Packaging Assay

Packaging was initiated, as detailed previously (4, 5), by bringing a microsphere carrying DNA into near contact with a microsphere carrying prohead-motor complexes in the presence of the standard packaging buffer containing 25 mM Tris-HCl, pH 7.5, 50 mM NaCl, 5 mM $MgCl_2$, and 0.5 mM ATP. Complexes were stalled by introducing a buffer containing 25 mM Tris-HCl, pH 7.5, 50 mM NaCl, 5 mM $MgCl_2$, and 0.4 mM ATPγS via a capillary tube, and were restarted by re-introducing standard packaging buffer. Measurements were made at ~23°C.

4. Data Analysis

The tether length was computed from the measured force vs. fractional extension relationship and velocities were calculated by linear fits to DNA tether length vs. time in a 3-s sliding window. The index of dispersion in normalized velocity for each ensemble was calculated in 5% filling bins by taking the variance of each bin divided by its mean. The % change in instantaneous velocity after stalling was calculated as $(V_{poststall} - V_{prestall}) / V_{prestall}$, with $V_{prestall}$ and $V_{poststall}$ determined from the last and first points, respectively, of linear trend lines fits to the 25 velocity data points before and after each stalling event, as shown in Fig1C of the main text. All error bars were determined by bootstrap analysis (7).

Pauses in which the motor temporarily stops translocating DNA for ~1-10 s are often observed (6). To score pausing events automatically we employed a residence time histogram method similar to that described previously (7). Histograms of residence time vs. tether length packaged in bins of 5% of the genome length were constructed for each packaging record and pauses were identified as peaks in these histograms exceeding a threshold determined from an equally sized ensemble of simulated packaging events not containing pauses. The median residence time within each bin was used for comparison to simulated data. Simulated packaging traces were generated according to the model described in Ref. (7) with added instrument noise measured experimentally. The average duration and frequency of pauses as a function of the % of the genome length packaged for each ensemble were calculated in 5% genome length bins and error bars were determined by bootstrap analysis (8).

C. Results

1. Acceleration of DNA packaging after long stalls

We measured the packaging of single DNA molecules into single phage phi29 proheads using a modified version of the optical tweezers technique described previously (10, 13) (see also Materials and Methods). Briefly, complexes consisting of the prohead with bound gp16 ATPase motor are attached to one microsphere and DNA molecules are attached to a second microsphere. When the DNA is brought into contact with the motor in the presence of ATP, packaging initiates and the DNA is translocated into the prohead (Fig. 2.1A). Packaging measurements were made with an applied 5 pN force,

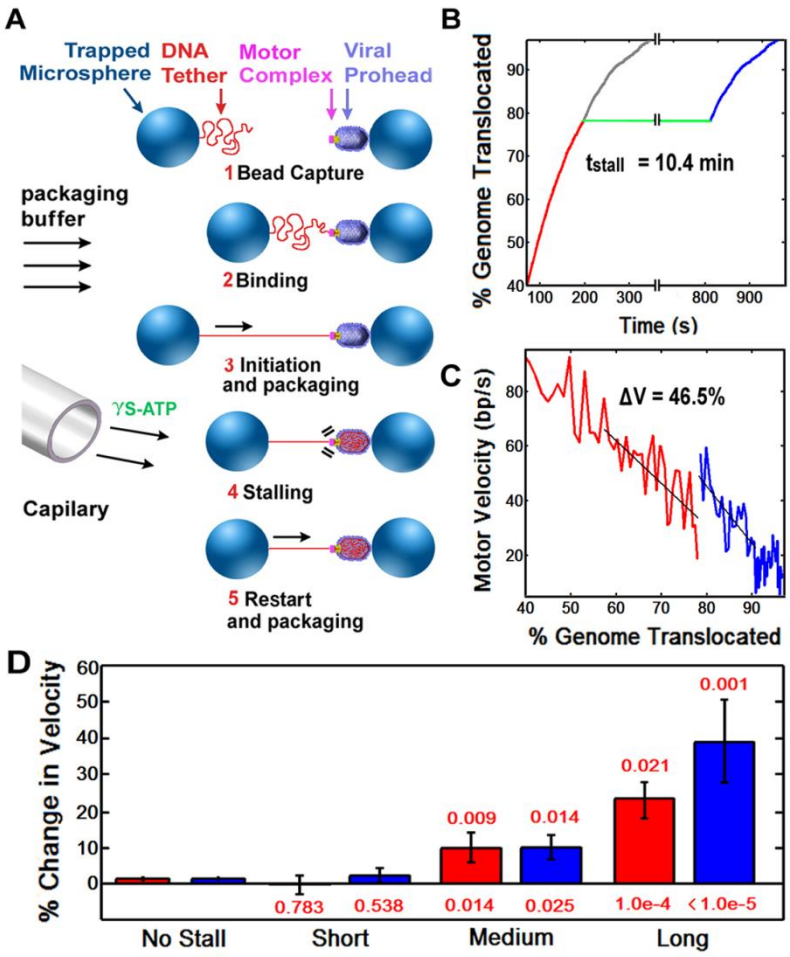

Figure 2.1. Motor stall-restart experiments. (A) Schematic diagram illustrating the experimental method. Packaging is initiated and followed to ~75% prohead filling under a low applied force (5 pN) (steps 1-3). The motor is then stalled by locally injecting the non-hydrolyzable analog γS-ATP via a micro-capillary tube (step 4). After a variable waiting time packaging is restarted by reintroducing ATP (step 5).
(B) Example packaging trajectory before (red) and after (blue) an imposed stall of 11.6 minutes. The grey plot shows the same data as in blue shifted back to the time of the stall, showing the acceleration. **(C)** Packaging rate vs. length of DNA packaged before (red) and after (blue) stalling for the event shown in (B). Black lines are linear trend lines fit to data before and after the stall point. **(D)** Mean change in packaging rate (blue) and motor velocity (red, rate not including pauses and slips) after short stalls (<3.4 min, average=1.5 min, n=50 events), medium stalls (3.4-10 min, average=5.7 min, n=50), and long stalls (>10 min, average=12.3 min, n=20). The bars marked "No Stall" indicate control experiments where the motor was not stalled (n=65). P-values for significance of differences vs. the next lowest stall time are indicated above the bars, and P-values for significance of differences vs. the no stall control are indicated below the bars.

which is small compared with the maximum force the motor can exert (>60 pN). The phi29 motor slows as packaging proceeds due to building forces resisting DNA confinement.

To test for nonequilibrium dynamics, we developed a new method (Fig. 2.1A) in which packaging was initiated and followed to ~75% prohead filling, where the motor has slowed significantly (9, 10, 13). We then stall the motor with non-hydrolyzable ATP and, after an imposed waiting time, restart packaging by re-introducing ATP. If the DNA were in a nonequilibrium state one would expect it to relax during the stall towards a lower energy state, thus presenting less resistance and, enabling the motor to accelerate upon restarting.

Indeed, measurements revealed clear increases in packaging rate upon restarting, providing direct evidence for nonequilibrium dynamics. A typical example is shown in Fig. 2.1B&C where the rate increased 47% after a 10.4 minute long stall. The average changes in packaging rate and motor velocity (rate not including pauses and slips, $\langle \Delta v \rangle$) clearly increase with increasing stall time (Fig. 2.1D). That both quantities exhibit significant changes illustrates that the acceleration is due mostly to a change in the inherent motor velocity, not just due to decreases in pausing and slipping. As a control, the same analysis procedure applied to events without induced stalls revealed no change in motor velocity, on average. This test shows that the observed accelerations following stalls are not simply due to normal fluctuations in motor velocity. Measurements after stalling at <50% filling also show no acceleration ($\langle \Delta v \rangle$=-4%; n= 85), indicating that nonequilibrium effects only have a measurable effect when the DNA is densely packed.

The observed acceleration after stalling implies a reduction in load on the motor due to relaxation of the DNA to lower energy conformations presenting lower resistance. We note that our previous studies employed the measured velocity vs. applied force relationship to infer an effective "internal force" resisting packaging (9, 10, 13). However, recent studies indicate that while both prohead filling and applied force slow the motor, they have a different influence on the detailed motor stepping kinetics and thus cannot be directly equated (31). Here, we refer to "resistance" or "load" on the motor as any interaction between the packaged DNA and motor which slows packaging.

The increasing trend of $\langle \Delta v \rangle$ with increasing stall time indicates that 10 minutes is a lower bound on the DNA relaxation time. Longer stalls were attempted, but we found measurements of the motor restart could rarely be obtained. The finding that nonequilibrium conformations persist for longer than it takes to package the entire genome (~6.6 min, on average) implies that the DNA can become kinetically trapped in an inherently nonequilibrium or "glassy" state. Thus, packaging is a dissipative process in which the motor must do more work than if the DNA was able to continuously relax to a minimum energy state.

2. Heterogeneous dynamics

Another expected consequence of nonequilibrium dynamics is heterogeneity in the dynamics of individual complexes. To investigate this we analyzed an ensemble of packaging events without imposed stalls (Fig. 2.2A). Inherent variability in packaging rate is expected even in the absence of a load due to stochastic motor kinetics; at low filling this is characterized by a constant index of dispersion (variance in motor velocity divided by mean velocity), as shown by detailed studies of the motor function (32).

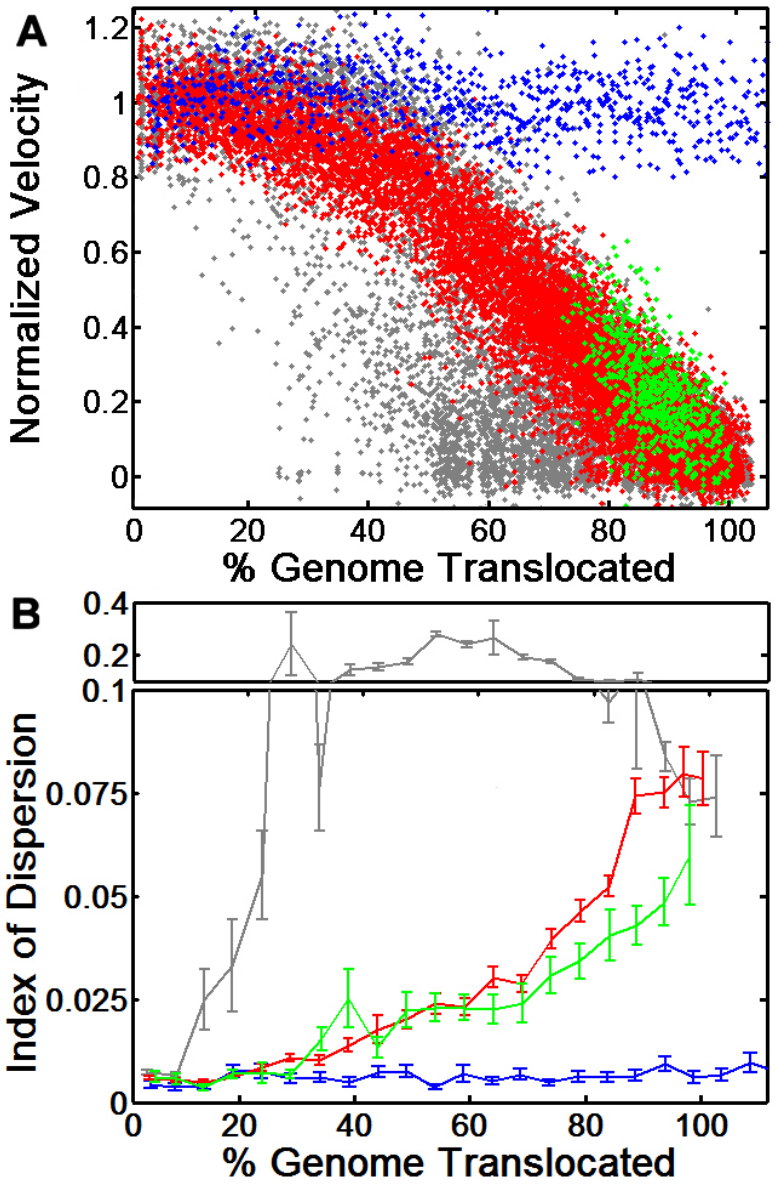

Figure 2.2. Heterogeneity in packaging dynamics. (A) Normalized velocities measured in 3 second intervals vs. filling measured for an ensemble of packaging events (red, n=85), events with perforated proheads (blue, n=58), events measured after long stalls (green, n=20), and events with 5 mM added spermidine (grey, n = 53). The velocities are normalized by the average velocity measured with <10% genome length packaged. **(B)** Index of dispersion (variance divided by mean) of normalized velocity vs. filling, labeled with the same colors as in (A).

Consistent with this, we find a constant index of dispersion up to 40% filling, but observe a clear increase beyond this point to a final value ~10-fold higher than that at low filling (Fig. 2.2B). This increase in dispersion indicates that the heterogeneity is due to variability in resistance to DNA confinement between different individual complexes. This finding implies the DNA does not follow a single conformational pathway during packaging.

Two additional findings further support this conclusion. First, a small fraction of packaging events do not show the usual trend of velocity decreasing with filling and the motors translocate far past the genome length (Fig. 2.2A). We interpret these as cases where the prohead is perforated and the DNA leaks out, so there is no resistance to packaging. A similar effect was observed with phage lambda proheads lacking a stabilizing protein (11). Notably, for these events the dispersion did not increase with length of DNA translocated. Second, the dispersion is also reduced following imposed stalls (Fig. 2.2B), consistent with the reaction proceeding closer to equilibrium following relaxation of the packaged DNA.

3. Packaging with added spermidine 3^{+}dramtically increases heterogeneity in packaging rates

Our results imply that the DNA can reorganize during packaging, despite being confined at very high density. A question of interest is what physical factors influence the DNA mobility. It has been proposed that Coulomb sliding friction between DNA segments may play an important role at high filling densities (17). The measurements

described above were in conditions with Na+ and Mg2+ ions screening the DNA, where the interaction between closely packed segments is purely repulsive (4, 19).

We also analyzed packaging measurements with 5 mM of added Spermidine+3, which induces a partly attractive interaction between DNA segments (33). In this case, we find a much larger index of dispersion (Fig. 2.2D), indicating that this condition favors the trapping of highly nonequilibrium conformations. Thus we have shown that the magnitude of the nonequilibrium effect can be reduced (by allowing relaxation), or increased (by changing the nature of the DNA-DNA interaction). Notably, studies have also shown that spermidine can inhibit DNA ejection from phage heads (15, 34), consistent with the notion that the DNA is locked in a condensed conformation.

4. The duration and frequency of intrinsic motor pausing is reduced after long stalls

A previously observed, but unexplained feature in phi29, lambda, and T4 packaging is the occurrence of ~1-10 second pauses in DNA translocation (9, 11, 12). Pausing increases sharply at high filling (Fig. 2.2.3A), suggesting it is connected to build-up of resistance. However, since the pauses are transient it is clear that the average resistance is not sufficiently high to continuously stall the motor. It has been proposed, based on simulations, that pausing could be due to large fluctuations in resistance due to formation of local nonequilibrium DNA conformations that transiently block packaging (25, 35). Consistent with this prediction, we observe that the average pause duration increases significantly above ~70% filling (Fig. 2.2.3A), suggesting conformations that temporarily prevent packaging relax on a timescale that increases with packaged DNA

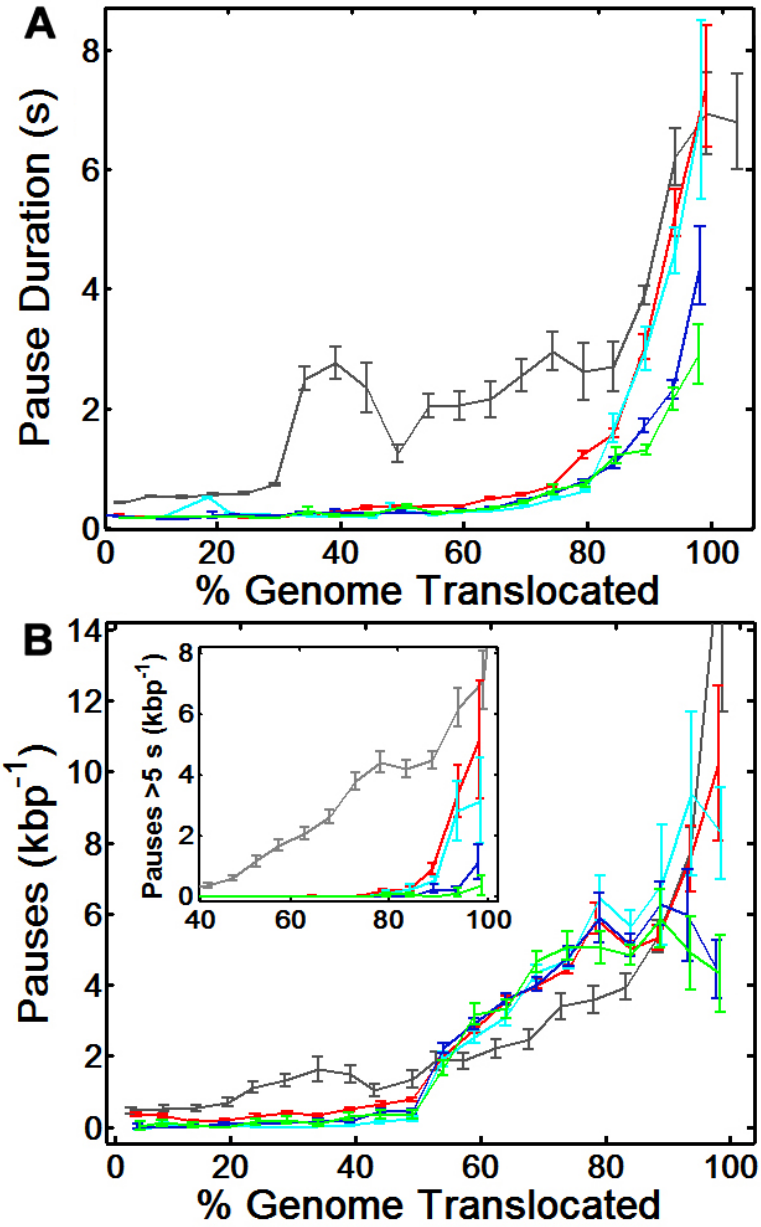

Figure 2.3. Motor pausing. (A) Pause duration and **(B)** Pause frequency per DNA length vs. filling for standard events (red), events with short stalls (light blue), medium length stalls (dark blue), and long stalls (green), and with 5 mM spermidine (grey). Inset shows frequencies of long pauses (> 5 s).

density. Notably, however, pause durations are much shorter than the >10 minute relaxation time revealed by our stall experiments. Thus, in our experiments there is evidence for two relaxation timescales: one associated with pauses lasting seconds, presumably corresponding to relaxation of locally jammed conformations, and a second associated with relaxation of the average resistance on a timescale >10 minutes, presumably corresponding to global relaxation.

We also observe a striking decrease in both frequency and duration of pauses following imposed stalls (Fig. 2.2.3), showing that pauses are associated with nonequilibrium conformations and suggesting that the two relaxation processes are experimentally coupled. Long pauses (> 5 s) are virtually eliminated following long stalls, further supporting the conclusion that DNA relaxation facilitates faster ongoing packaging via a closer-to-equilibrium conformational pathway. In addition, we observed virtually no pausing in the events where packaging did not slow with filling. In contrast, addition of spermidine causes a significant increase in the amount of time spent paused, consistent with increased trapping of the DNA in nonequilibrium conformations.

D. Discussion

1. The packaged DNA adopts a non-equilibrium structure at high filling

Our findings show that packaging cannot be fully understood by quasistatic thermodynamic models and support several hypotheses proposed based on dynamic simulations. Forrey and Muthukumar (25) predicted a significant influence of nonequilibrium DNA polymer dynamics on viral packaging. Specifically, consistent with

our findings, they predicted large heterogeneity in dynamics at >50% filling, large fluctuations in resistance forces, and pauses in DNA translocation. They attributed pauses to steric blockages due to local crowding of DNA segments and pause durations to relaxation dynamics of the confined DNA, predicted to adopt a nonequilibrium glassy structure at high filling.

2. Comparison with theoretical studies of DNA packaging

Ali et al. (27, 36) also predicted disordered conformations and pauses with durations that increase with filling due to fluctuations in resistance. Additionally, they predicted that the forces driving viral DNA ejection, occurring at a later time after packaging has finished when a virus infects the next cell, would be lower than the forces resisting packaging due to dissipative dynamics. The latter prediction is consistent with our finding that, when packaging is stalled, the DNA can relax to a conformation presenting less resistance. Petrov, Harvey, and co-workers (6, 30) also predicted varying conformations and resistance at high filling and the need for extensive equilibration to produce partially ordered structures. In addition, they predicted, from analysis of structural correlation functions, that the DNA would adopt a glassy state at high filling (31).

3. Comparison with structural data

Available experimental information on DNA structure in phi29 has come from cryo-electron microscopy studies in which 3D reconstructions are obtained by averaging a large ensemble of images of individual frozen particles (37, 38). Although early studies of the DNA conformation in phage T7 were interpreted as indicating a highly ordered

spool conformation of DNA based on the observation of distinct layers of average DNA density, later studies of other phages and modeling studies called the generality of this interpretation into question (26, 29). Comolli et al. (29) studied phi29 by cryo-electron microscopy with 3D reconstruction from ensembles of images of frozen particles. With a fully packaged genome, the arrangement of a central portion of DNA in the core was unresolved but five concentric layers of average DNA density adjacent to the prohead wall were observed, suggesting local close packing of segments in this region. However, reconstructions of partially packaged (32–78%) proheads showed uniform average DNA density throughout, consistent with heterogeneous DNA conformations.

4. Comparison to studies of polymer dynamics under tight confinement

Beyond having relevance to viral packaging, the behavior of polymers in confined geometries has long been a topic of fundamental interest in polymer physics (39–41) and, more recently, has attracted attention due to emerging applications of nanofabricated devices for DNA manipulation in biotechnology (42). Confinement of single DNA molecules in nanofabricated slits and channels has been extensively studied and shown to increase the molecular relaxation time due to reductions in conformational entropy and hydrodynamic interactions with the confining walls (42–44). Entropic penalties for confining flexible or worm-like polymers in slits, tubes, and spheres have recently been computed theoretically (45). Experimentally, in the most extreme cases reported, confinement of lambda DNA between two surfaces separated by 32 nm was shown to increase the molecular relaxation time ~30-fold (44), whereas confinement in a 140 × 130-nm channel caused a ~20-fold increase (42, 43). The effect of tight 3D confinement has not previously been experimentally studied but our results show that it causes more

dramatic effects. Specifically, the >10-min relaxation time revealed by our experiments is >60,000 times that for unconfined DNA of the same length (46).

The DNA concentration within phi29, like many other double-stranded DNA bacteriophages, is very high (~0.5 g/mL), and one would expect excluded volume and chain entanglements to strongly restrict molecular motion (39, 47, 48). The effect of entanglements on the dynamics of polymers in melts and concentrated solutions has been successfully predicted by reptation models, in which polymer motion is restricted to a tube-shaped region parallel to the chain contour (39, 49). Viral DNA packaging differs in several ways from the typical situations in which the reptation model is applied. Specifically, one end of the DNA is constrained by the motor, it is a highly charged polymer tightly confined in three dimensions, and at the highest densities it may form a variety of locally ordered liquid crystal-like phases (18, 50), all of which may further slow relaxation. Nevertheless, the notion that a reptation-like process may play a role in viral DNA packaging, or in the converse process of DNA ejection, has been discussed previously in a number of theoretical papers (18, 51–53). It has been proposed, for example, that the relaxation time predicted by reptation theory may set a lower bound on the relaxation time of the packaged DNA (54). The tube disengagement time in reptation theory is predicted to scale with polymer length (L) and concentration (c) as $\tau D \sim L^3 c^{1.5}$ (39). Studies in our laboratory indicate that $\tau_D \cong 40$ s for 115-kbp DNA at 1 mg/mL (49). For the length and concentration of DNA confined in the phi29 prohead at 75% filling, the theoretical scaling law would thus predict $\tau_D = 10.6$ min, a value consistent with the lower bound implied by our stall–restart measurements.

5. Conclusions

In summary, we report evidence for nonequilibrium dynamics of DNA during viral packaging that slows the motor, causes heterogeneity in packaging rates of individual viruses, and explains the frequent pausing observed in motor translocation. Because many viruses package DNA to similarly high density as phi29, it is likely that our findings are broadly applicable. Studies of several phages, including phi29, show that DNA is packaged in vivo (in the infected host cell) at similarly high rates as we measure *in vitro* (55⇓–57). Therefore, the nonequilibrium effects we report are likely relevant in vivo. Although fast packaging may result in higher mechanical work due to nonequilibrium forces, the motor is nevertheless strong enough to complete the process. Faster packaging also does not necessarily imply a higher energy requirement, because studies and models suggest that the motor uses the same amount of ATP per total length of DNA packaged regardless of load and packaging rate (33, 58). Our studies also provide unique experimental data to test theoretical models of viral packaging, and, more generally, theories for polymer dynamics under strong 3D confinement.

Chapter II, in full, is a reprint that the dissertation author was the principal researcher and author of. The material appears in *PNAS*. (**Z. T. Berndsen,** N. Keller, S. Grimes, P. J. Jardine, D. E. Smith. (2014). Nonequilibrium dynamics and ultraslow relaxation of confined DNA during viral packaging , *Proceedings of the National Academy of Science,* 111, 8345)

E. References

1. Riemer S.C. & Bloomfield V.A. (1978) Packaging of DNA in bacteriophage heads - some considerations on energetics. Biopolymers 17(3): 785-794.

2. Odijk T. (1998) Hexagonally packed DNA within bacteriophage T7 stabilized by curvature stress. Biophys J 75(3): 1223-1227.

3. Kindt J., Tzlil S., Ben-Shaul A. & Gelbart W.M. (2001) DNA packaging and ejection forces in bacteriophage. Proc Natl Acad Sci U S A 98(24): 13671-13674.

4. Tzlil S., Kindt J.T., Gelbart W.M. & Ben-Shaul A. (2003) Forces and pressures in DNA packaging and release from viral capsids. Biophys J 84(3): 1616-1627.

5. Purohit P.K., Kondev J. & Phillips R. (2003) Mechanics of DNA packaging in viruses. Proc Natl Acad Sci U S A 100(6): 3173-3178.

6. Harvey S.C., Petrov A.S., Devkota B. & Boz M.B. (2009) Viral assembly: A molecular modeling perspective. Phys Chem Chem Phys 11(45): 10553-10564.

7. Smith D.E. (2011) Single-molecule studies of viral DNA packaging. Curr Opin Virol 1: 134.

8. Feiss M. & Rao V.B. (2012) in Viral Molecular Machines, (Springer, pp 489-509.

9. Smith D.E., Tans S.J., Smith S.B., Grimes S., Anderson D. L. & Bustamante C. (2001) The bacteriophage phi29 portal motor can package DNA against a large internal force. Nature 413(6857): 748-752.

10. Fuller D.N, Rickgauer J.P., Grimes S., Jardine P.J., Anderson D., Smith D. E (2007) Ionic effects on viral DNA packaging and portal motor function in bacteriophage phi 29. Proc Natl Acad Sci U S A 104(27): 11245-11250.

11. Fuller D.N., Raymer D.M., Rickgauer J.P., Robertson R.M., Catalano C.E., Anderson D.L., Grimes S., Smith D.E. (2007) Measurements of single DNA molecule packaging dynamics in bacteriophage lambda reveal high forces, high motor processivity, and capsid transformations. J Mol Biol 373(5): 1113-1122.

12. Fuller DN, Raymer DM, Kottadiel VI, Rao VB & Smith DE (2007) Single phage T4 DNA packaging motors exhibit large force generation, high velocity, and dynamic variability. Proc Natl Acad Sci U S A 104(43): 16868-16873.

13. Rickgauer, J. P., Fuller D.N., Grimes S., Jardine P.J., Anderson D., Smith D. E. (2008) Portal motor velocity and internal force resisting viral DNA packaging in bacteriophage phi29. Biophys J 94(1): 159-167.

14. Tsay J.M., Sippy J., Feiss M. & Smith D.E. (2009) The Q motif of a viral packaging motor governs its force generation and communicates ATP recognition to DNA interaction. Proc Natl Acad Sci U S A 106(34): 14355-14360.

15. Evilevitch A., Lavelle L., Knobler C.M., Raspaud E. & Gelbart W.M. (2003) Osmotic pressure inhibition of DNA ejection from phage. Proc Natl Acad Sci U S A 100(16): 9292-9295.

16. Arsuaga J., Tan R.K., Vazquez M., Sumners D.W. & Harvey S.C. (2002) Investigation of viral DNA packaging using molecular mechanics models. Biophys Chem 101: 475-484.

17. Odijk T. (2004) Statics and dynamics of condensed DNA within phages and globules. Phil Trans Roy Soc A 362(1820): 1497-1517.

18. Metzler R. & Dommersnes P.G. (2004) Helical packaging of semiflexible polymers in bacteriophages. European Biophysics Journal 33(6): 497-505.

19. Purohit P.K., Inamdar M. M., Grayson P. D., Squires T. M., Kondev J., Phillips R. (2005) Forces during bacteriophage DNA packaging and ejection. Biophys J 88(2): 851-866.

20. Klug W, Feldmann M & Ortiz M (2005) Three-dimensional director-field predictions of viral DNA packing arrangements. Comput Mech 35(2): 146-152.

21. Cerritelli M.E., Cheng N., Rosenberg A.H., McPherson C.E., Booy F.P., Steven A.C. (1997) Encapsidated conformation of bacteriophage T7 DNA. Cell 91(2): 271-280.

22. Qiu X., Rau D.C., Parsegian V.A., Fang L.T., Knobler C.M., Gelbart W.M. (2011) Salt-dependent DNA-DNA spacings in intact bacteriophage λ reflect relative importance of DNA self-repulsion and bending energies. Phys Rev Lett 106(2): 028102.

23. LaMarque J.C., Le T.L. & Harvey S.C. (2004) Packaging double-helical DNA into viral capsids. Biopolymers 73(3): 348-355.

24. Spakowitz A.J. & Wang Z.G. (2005) DNA packaging in bacteriophage: Is twist important?. Biophys J 88(6): 3912-3923.

25. Forrey C. & Muthukumar M. (2006) Langevin dynamics simulations of genome packing in bacteriophage. Biophys J 91(1): 25-41.

26. Ali I., Marenduzzo D. & Yeomans J.M. (2006) Polymer packaging and ejection in viral capsids: Shape matters. Phys Rev Lett 96(20): 208102.

27. Petrov A.S. & Harvey S.C. (2007) Structural and thermodynamic principles of viral packaging. Structure 15(1): 21-27.

28. Comolli L.R., Spakowitz A.J., Siegerist C.E., Jardine P.J., Grimes S., Anderson D.L., Bustamante C., Downing K.H. (2008) Three-dimensional architecture of the bacteriophage phi29 packaged genome and elucidation of its packaging process. Virology 371(2): 267-277.

29. Petrov A.S. & Harvey S.C. (2008) Packaging double-helical DNA into viral capsids: Structures, forces, and energetics. Biophys J 95(2): 497-502.

30. Petrov A.S., Locker C.R. & Harvey SC (2009) Characterization of DNA conformation inside bacterial viruses. Phys Rev E 80(2): 021914.

31. Liu S., Chistol G., Hetherington C.L., Tafoya S., Aathavan K., Schnitzbauer J., Grimes S., Jardine P.J., Bustamante C. (2014) A viral packaging motor varies its DNA rotation and step size to preserve subunit coordination as the capsid fills. Cell 157

32. Moffitt J.R., Chemla Y.R., Aathavan K., Grimes S., Jardine P.J., Anderson D.L., Bustamante C. (2009) Intersubunit coordination in a homomeric ring ATPase. Nature 457(7228): 446-450.

33. Bloomfield V.A. (1997) DNA condensation by multivalent cations. Biopolymers 44(3): 269-282.

34. Evilevitch A. (2006) Effects of condensing agent and nuclease on the extent of ejection from phage λ. J Phys Chem B 110(44): 22261-22265.

35. Ali I., Marenduzzo D. & Yeomans J.M. (2004) Dynamics of polymer packaging. J Chem Phys 121(17): 8635-8641.

36. Nelson R.A., Reilly B.E. & Anderson D.L. (1976) Morphogenesis of bacteriophage phi 29 of bacillus subtilis: Preliminary isolation and characterization of intermediate particles of the assembly pathway. J Virol 19(2): 518-532.

37. Laemmli U.K. & Favre M. (1973) Maturation of the head of bacteriophage T4: I. DNA packaging events. J Mol Biol 80(4): 575-599.

38. Black L.W. & Silverman D.J. (1978) Model for DNA packaging into bacteriophage T4 heads. J Virol 28(2): 643-655.

39. Chemla Y.R., Aathavan K., Michaelis J., Grimes S., Jardine P.J., Anderson D.L., Bustamante C. (2005) Mechanism of force generation of a viral DNA packaging motor. Cell 122(5): 683-692.

40. Xiang Y., Morais M.C., Battisti A.J., Grimes S., Jardine P.J., Anderson D.L., Rossmann M.G. (2006) Structural changes of bacteriophage phi29 upon DNA packaging and release. EMBO J 25(21): 5229-5239.

41. Tang J., Olson N., Jardine P.J., Grimes S., Anderson D.L., Baker T.S. (2008) DNA poised for release in bacteriophage phi29. Structure 16(6): 935-943.

42. De Gennes P.G. (1979) Scaling Concepts in Polymer Physics, (Cornell University Press, Ithaca, NY),

43. Odijk T. (1993) Physics of tightly curved semiflexible polymer chains. Macromolecules 26(25): 6897-6902.

44. Sakaue T. (2007) Semiflexible polymer confined in closed spaces. Macromolecules 40(14): 5206-5211.

45. Reisner W., Pedersen J.N. & Austin R.H. (2012) DNA confinement in nanochannels: Physics and biological applications. Rep Prog Phys 75(10): 106601.

46. Reisner W., Morton K.J., Riehn R., Wang Y.M., Yu Z., Rosen M., Sturm J.C., Chou S.Y., Frey E., Austin R.H. (2005) Statics and dynamics of single DNA molecules confined in nanochannels. Phys Rev Lett 94(19): 196101.

47. Tang J., Levy S. L., Trahan D. W., Jones J.J., Craighead H.G. and Doyle P.S. (2010) Revisiting the conformation and dynamics of DNA in slitlike confinement. Macromolecules 43(17): 7368-7377.

48. Smyda M.R. & Harvey S.C. (2012) The entropic cost of polymer confinement. J Phys Chem B 116(35): 10928-10934.

49. Perkins T.T., Quake S.R., Smith D.E. & Chu S. (1994) Relaxation of a single DNA molecule observed by optical microscopy. Science 264(5160): 822-826.

50. Robertson R.M. & Smith D.E. (2007) Self-diffusion of entangled linear and circular DNA molecules: Dependence on length and concentration. Macromolecules 40(9): 3373-3377.

51. Robertson R.M. & Smith D.E. (2007) Strong effects of molecular topology on diffusion of entangled DNA molecules. Proc Natl Acad Sci U S A 104(12): 4824-4827.

52. Robertson R.M. & Smith D.E. (2007) Direct measurement of the intermolecular forces confining a single molecule in an entangled polymer solution. Phys Rev Lett 99(12): 126001.

53. Leforestier A. & Livolant F. (2010) The bacteriophage genome undergoes a succession of intracapsid phase transitions upon DNA ejection. J Mol Biol 396(2): 384-395.

54. Gabashvili I.S. & Grosberg A.I. (1991) Bacteriophage DNA reptation. Biofizika 36(5): 788-793.

55. Gabashvili I.S. & Grosberg A.Y. (1992) Dynamics of double stranded DNA reptation from bacteriophage. Journal of Biomolecular Structure and Dynamics 9(5): 911-920.

56. Inamdar M.M., Gelbart W.M. & Phillips R. (2006) Dynamics of DNA ejection from bacteriophage. Biophys J 91(2): 411-420.

57. Marenduzzo D. (2008) Computer simulations of DNA packing inside bacteriophages: Elasticity, electrostatics and entropy. Computational and Mathematical Methods in Medicine 9(3-4): 317-325.

58. Marenduzzo D. (2009) Statistics of confined polymers and the melting of a DNA spool. EPL (Europhysics Letters) 85(3): 38005.

59. Zhao W., Morais M.C., Anderson D.L., Jardine P.J. & Grimes S. (2008) Role of the CCA bulge of prohead RNA of bacteriophage ø29 in DNA packaging. J Mol Biol 383(3): 520-528.

60. Peroutka III R.J., Orcutt S.J., Strickler J.E. & Butt T.R. (2011) in Heterologous Gene Expression in E. coli, (Springer, NY, NY), pp 15-30.

61. Fuller D.N., Gemmen G.J., Rickgauer J.P., Dupont A., Millin R., Recouvreux P., and Smith D.E. (2006) A general method for manipulating DNA sequences from any organism with optical tweezers. Nucleic Acids Res 34(2): e15.

62. Rickgauer J.P., Fuller D.N. & Smith D.E. (2006) DNA as a metrology standard for length and force measurements with optical tweezers. Biophys J 91(11): 4253-4257.

Chapter III

Continuous Allosteric Regulation of a Viral Packaging Motor by a Sensor that Detects Density and Conformation of the Packaged DNA

A. Introduction

A critical step in the assembly of many dsDNA viruses is the packaging of the viral genome into preformed prohead shells (1-4). In phage phi29, a 19.3 kbp genome is packaged into a 42×54 nm prohead via a ~4 nm diameter portal channel (5). This channel is comprised of a ring of portal proteins (gene product 10, gp10, also referred to as the head-tail "connector"). A ring of the packaging motor proteins (gp16) docks to the portal on the exterior of the prohead via an intervening ring of RNA molecules (prohead RNA, pRNA) (Fig. 3.1). Gp16 converts chemical energy from ATP hydrolysis into mechanical work to translocate the DNA through the portal. This is a remarkable process because near-crystalline packing density of the DNA is achieved against large resistance forces anticipated to arise from DNA bending rigidity, electrostatic self-repulsion of DNA segments, and entropy loss (6-10).

The dynamics of DNA translocation and forces generated by the molecular motor have been measured in the bacteriophage phi29, lambda, and T4 systems via single DNA molecule manipulation with optical tweezers (11-22). Two striking observations observed in both phi29 and lambda are that the motor velocity decreases sharply with increasing prohead filling and also decreases with increasing externally applied force (11, 14, 16).

Recently, we showed that the DNA inside phage phi29 undergoes nonequilibrium dynamics during packaging, which slows the motor, causes heterogeneity in packaging rates of individual viruses, and causes frequent pauses in motor translocation (23). At high prohead filling we showed that the DNA adopts a nonequilibrium conformation that relaxes on a timescale >10 minutes, which is longer than the packaging reaction (~6.6

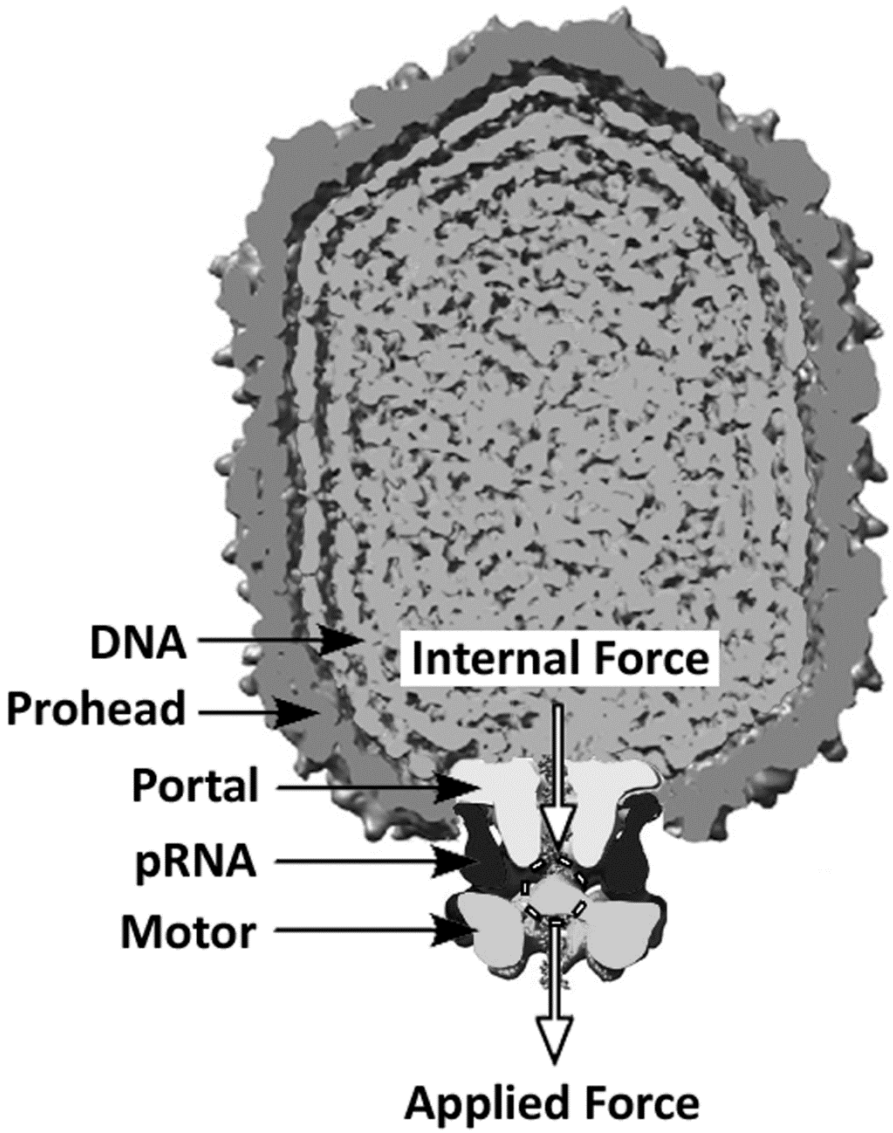

Figure 3.1. Components of the phi29 packaging complex. Arrangement of the packaging components based on superposition of the cryoEM structure of the portal-pRNA-motor complex (after Ref. (24)) onto that of the fully packaged virus (after Ref.(25)). The arrows schematically illustrate that both internal and applied forces exert loads on the motor at the site where the motor grips the DNA, opposite to the direction of translocation. Note: the dimensions of the prohead shell are 42×54 nm.

minutes, on average). The observed heterogeneity in packaging rates indicates that the DNA packaged in different individual viruses adopts different conformations and that the motor velocity depends not only on the length of DNA packaged, but also its conformation.

We report here that the amount of DNA inside the prohead, as well as its conformation, also indirectly influence motor function in a manner that is distinct from the influence of the forces resisting DNA confinement that directly load the motor. Much of the decrease in motor velocity with filling is attributable to this effect. Since only part of the slowing can be attributed to load forces, our present findings show that the previous analysis based on an assumption that load force was the only factor slowing the motor overestimated the resisting forces (11, 13, 16). Detailed measurements of motor slipping presented here suggest the force resisting DNA confinement is quite low until ~70% filling, but then builds rapidly during the final stages of packaging. The surprising implication of these findings is that the motor, besides being directly affected by load force, is also indirectly regulated by an allosteric interaction between the DNA packaged inside the prohead and the motor mounted on the outside. We further show that these findings are consistent with recent studies demonstrating highly coordinated burst-dwell stepping kinetics of the packaging motor (26).

B. Materials and Methods

1. Biochemical Reagents

Phi29 components were provided by Dr. Shelley Grimes and Dr. Paul Jardine and prepared as described previously (23). Briefly, for bacteriophage phi29 packaging components, fiberless proheads were produced by infection of *B. subtilis* 12A (*sup*-) with the ø29 mutant *sus* 8.5(900)-16(300)-14(1241) (defective in head fibers and the packaging ATPase) and purified as described previously (1). The packaging ATPase was produced from the plasmid pSACB-gp16 in *B. subtilis* and purified by chromatography as described previously (1), or produced as a fusion protein in the SUMO Pro vector (LifeSensors, Inc, Malvern, PA) and expressed in *E. coli* (2). The SUMO tag was subsequently cleaved off and removed by IMAC, yielding non-tagged ATPase. A 25 kbp dsDNA packaging substrate labeled at one end with biotin was prepared by PCR, as described previously (3), from a stock solution of lambda phage DNA using primers biotin- CTGATGAGTTCGTGTCCGTACAACTGGCGTAATC and aminoC_6-digoxigenin-ATCCGATCTGCGTTACCGAATGGATGGATG (Operon Inc.). This DNA was tethered to 2.8 μm diameter streptavidin coated microspheres as described previously (4, 5). Procapsid-motor complexes were pre-assembled and attached via anti-phi29 antibodies to 2.1 μm protein G coated microspheres as described previously (4, 5).

2. Optical Tweezers

Two measurement modes were used. In the "force-clamp" mode, the applied tension is held constant at a preset value by use of feedback control system that adjusts the separation between the two traps. In the "fixed trap position" mode, the tension is allowed to build as packaging proceeds. The tweezers were calibrated as described previously (28, 29). The tether length was computed from the measured force vs. fractional extension relationship and all velocities were calculated by linear fits to DNA

tether length vs. time in a 3-s sliding window. All error bars were determined by bootstrap analysis.

3. Single Molecule Packaging Assay and nucleotide exchange experiments

Packaging was initiated by bringing a microsphere carrying DNA into near contact with a microsphere carrying prohead-motor complexes in the presence of the standard packaging buffer containing 25 mM Tris-HCl, pH 7.5, 50 mM NaCl, 5 mM MgCl2 with 0.5 mM ATP, as described previously (13, 16). Exchange between solutions containing ATP and γS-ATP was achieved using a custom made microfluidic flow cell. Measurements were conducted in a channel filled with gently flowing ATP solution. The flow cell was attached to a translation stage, allowing a tethered complex held fixed in the laboratory frame by the optical traps to be rapidly moved near the end of a capillary tube delivering a 0.4 mM γS-ATP solution in the same background buffer, causing rapid (<1 s) solution exchange and stalling the motor. The motor was then restarted by moving the complex away from the capillary tube and back into the flowing ATP solutions, again achieving nearly instant solution exchange. Measurements were made at ~23°C.

4. Data Analysis

The tether length was computed from the measured force vs. fractional extension relationship and all velocities were calculated by linear fits to DNA tether length vs. time in a 3-s sliding window. All error bars were determined by bootstrap analysis.

Pauses in which the motor temporarily stops translocating DNA for ~1-10 s and slips in which segments of DNA rapidly exit the prohead are often observed (11). To

score pausing events automatically we employed a residence time histogram method described previously (18). Slips were scored for both fixed-force and fixed-position measurements as any increase in DNA tether length that occurred within ~1s and were larger than a threshold determined from an equally sized ensemble of simulated packaging events not containing slips. Simulated packaging traces were generated according to the model described in Ref. (18), with added instrument noise as measured experimentally. The average frequency of pauses and slips as functions of the % of the genome length packaged for each ensemble were calculated in 5% genome length bins.

5. Simulations of the phi29 packaging motor.

i. The mechanochemical model

To model the phi29 packaging motor a 3-state chemical reaction scheme was chosen as described in Ref. (50). In this model, each subunit hydrolyses one ATP molecule following the chemical reaction cycle

$$E \rightarrow T \rightarrow D \rightarrow E$$

Where E,T, and D represent the empty (apo), ATP bound, and ADP bound states respectively. A more complete description in accord with current understandings could include both an ATP tight binding state, T^*, and a phosphate bound state, EP_i, as well as an off pathway γS-ATP bound state and an off-pathway paused state, however the three state model dramatically simplifies the simulation procedure as the number of chemical states scales as n^m where n is the number of states per subunit and m is the number of subunits. Although there is still some debate about the stoichiometry of the packaging motor, the most widely agreed upon model is that the gp16 ATPase forms a homo-

pentameric ring, which will be labeled $S_1S_2S_3S_4S_5$. According to detailed high resolution measurements published over the last decade by the Bustamante lab at UC Berkeley (20,26, 49), the following dominant mechanochemical cycle can be constructed, starting from the all T state and assuming physiological substrate concentrations (5 μM Pi, 5 μM ADP, and 250 μM ATP):

TTTTT > DTTTT > DDTTT > DDDTT > DDDDT > DDDDD > EDDDD > TDDDD > TEDDD > TTDDD > TTEDD > TTTDD > TTTED > TTTTD > TTTTE > TTTTT

In this scheme, the 2nd-4th *T-D* transitions produce a 2.5 bp step while the first *T-D* serves to initiate the hydrolysis cascade around the ring without generating a step. This is a requirement given the fact that only four 2.5bp steps/ cycle are observed and are always observed to occur in rapid succession, even at very low ATP concentrations. This produces what is referred to as a burst-dwell cycle. Again, detailed analysis of this reaction has shown that the dwell phase consists of ADP unbinding and ATP binding occurring in an interlaced fashion followed by the first hydrolysis and phosphate release which initiates a rapid hydrolysis cascade that proceeds sequentially around the ring in an accelerated fashion due to arginine finger catalysis by the neighboring subunit, with each 2.5bp step accompanying a phosphate release transition. Probably the most complicated and confusing aspect of this model has to do with the role being played by the subunit that does not appear to produce a step, which is referred to as the “special subunit.” In

this model, the special subunit is the first to hydrolyze ATP and the first to release its ADP at the start of the dwell phase. This conclusion was reached by a detailed analysis of the stepping statistic immediately preceding long stalls in packaging induced by γS-ATP binding to one of the five subunits and is favored by symmetry constraints as well. In the 3-state model the *T-D* transition generates the 2.5 bp substeps. In addition, it is now understood that ADP release events are the rate limiting transitions at low filling and saturating ATP concentrations with one ADP release rate being slightly different than the other four. Finally, it has been shown (49) that only the burst phase is influenced by applied force, not the dwell, with the waiting time between each 2.5 bp step lengthening as the force acting on the motor in the direction opposite packaging increases, implying that Pi release is the force generating transition, whereas hydrolysis serves to break the strong DNA-gp16 contacts allowing translocation to occur.

ii. Monte Carlo simulations

Stochastic simulations of phi29 packaging were carried out largely according to the procedure described in Ref. (50) which is an implementation of the algorithm described in Ref. (51). In this model the motor is treated as a source of translocating force and a Langevin equation of motion is derived for the DNA in terms of its packaging distance $z(t)$ only (disregarding rolling and rotational degrees of freedom). This Langevin equation predicts the time evolution of a single stochastic trajectory of the system; however it is more useful here to look at the time evolution of the probabilities of the different states of the system. This is accomplished by transforming the Langevin equation into an equivalent Fokker-Planck equation of the form (50,51),

$$\frac{\partial \rho_j}{\partial t} = \underbrace{\frac{D}{k_B T}\frac{\partial}{\partial z}\left[\left(\frac{\partial}{\partial z}V^j_{eff}(z) + F_L\right)\rho_j\right]}_{\text{Translocation and load forces}} + \underbrace{D\frac{\partial^2 \rho_j}{\partial z^2}}_{\text{Brownian motion}} + \underbrace{\sum_i k_{ji}(z)\rho_i}_{\text{Chemical reactions}}$$

describing the time evolution of the probability densities of the different states of the system. V^j_{eff} is the potential in direction z, and D is the diffusion constant. Here, the first term on the right describes translocation and load forces, the second term described Brownian motion, and the third term describes the Markov transitions among different chemical states. In this model the load force is absorbed into the potential term. For molecular motors where every power stroke is regarded as identical the potential, V is periodic. For phi29 this potential repeats every 2.5 bp in the z direction as the DNA is passed from one subunit to the next. The exact form of the potential is not known, however because the transitions are thermally activated, the exact form is not important and can be modeled by $\sin^2$ functions (50). Ref. (51) outlines a "finite volume" procedure for solving the Fokker-Planck equation that relates the continuum model to a discrete mechanochemical kinetic model. The master equation for the jump process takes the form (50, 51),

$$\frac{dp^j_i}{dt} = \underbrace{(p^j_{i-1}r^j_{i-1\to i} - p^j_i r^j_{i\to i-1}) - (p^j_i r^j_{i\to i+1} - p^j_{i+1}r^j_{i+1\to i})}_{\text{Spatial transitions}} + \sum_{j'\neq j}\underbrace{(p^{j'}_i r^{j'\to j}_i - p^j_i r^{j\to j'}_i)}_{\text{Chemical transitions}}.$$

where the r terms represent spatial and chemical transition rates and are the two terms necessary to uniquely specify a steady-state solution. Yu et.al use this method to derive the following rate equations (50) for each transition in the 3-state hydrolysis model and individual trajectories are generated with the kinetic Monte Carlo algorithm (52).

$$k_{E\to T} = k^0_{E\to T}\cdot[ATP]$$
$$k_{T\to E}(z) = k^0_{T\to E}\cdot\exp[\Delta V_T(z) - \Delta V_E(z)]$$
$$k_{T\to D}(z) = k^0_{T\to D}\cdot\exp[\Delta V_T(z) - \Delta V_D(z)]$$
$$k_{D\to T} = k^0_{D\to T}\cdot[Pi]$$
$$k_{D\to E}(z) = k^0_{D\to E}\cdot\exp[\Delta V_D(z) - \Delta V_E(z)]$$
$$k_{E\to D} = k^0_{E\to D}\cdot[ADP]$$

This algorithm assumes all transitions are Poisson processes and the first passage time is calculated as $t_{draw} = -(1/k)ln(r)$, where r is a random number on the interval (0,1) and k is the sum of the rate constants of all possible transitions out of the current state. The high resolution packaging data (20,26,49) indicate that the spatial and chemical transitions of the phi29 packaging motor are very tightly coupled (ie deviations from the dominant mechanochemical reaction scheme, in which the DNA moves in steps of 2.5 bp in the direction of packaging coupled to ATP hydrolysis and phosphate release by one subunit, occur with negligibly low frequency) and we now know that opposing forces remain low and constant throughout most of the packaging reaction such that they have a negligible effect on the packaging rate until very high filling. In light of this I found it was possible to simplify the model even further by removing the potential term all together and simulating chemical transitions only and still produce very similar results as those presented in Ref. (50). Therefore in my model all $V(z)$ dependent terms are removed and only concentration terms remain to modify the standard condition rate constants. In this model the DNA-motor interactions are ignored and the *T-D* transition is always accompanied by a 2.5 bp step. To incorporate the effect of load force, the *T-D* transition rate was set to match the experimentally determined burst-duration vs. external

force relationship (26, 49), such that k_{TD}(F)= Burst Duration(F)/4. To account for removing the $\Delta\Delta V(z)$ term I tuned the ratio of the forward and backward rates such that the free energy change ($k_{ij}/k_{ji} = \exp(\Delta G/k_B T)$) at experimental conditions closely matched those reported in Ref. (50).

iii. Setting rate constants at low force and low filling

The procedure followed for tuning the standard condition rate constants was based largely on that outlined in Ref. (50) and the parameters found to best reproduce all experimental data are shown in table 3.1. Numerous constraints can be constructed to reduce the parameter space of plausible values for the rate constants, the most important of which is that of detailed balance. For chemical systems, general features describing the behavior of the system at equilibrium *($\Delta G = 0$, $k_{ij} = k_{ji}$)* can be used to understand the dynamics of the system when it is out of equilibrium, as is always the case for molecular motors operating under physiological conditions within the cellular environment. For instance, at equilibrium the fractional population of units in state *i*, X_i, is proportional to $exp(-G_i/k_BT)$ where G_i is the free energy of state *i*. For every pair of connected states (*i* and *j*) the number of forward crossings must equal the number of backwards crossings on average. Since the number of crossings is proportional to the fractional population times the rate constant the following relations are established

$$X_i k_{ij} = X_j k_{ji} \quad \text{and} \quad k_{ij}/k_{ji} = exp(\Delta G_{ij}/k_B T)$$

with ΔG_{ij} being composed of both the standard condition free energy change (ΔG^o) and a term that depends on the concentrations of whatever reactants are involved in that particular transition. For a molecular motor which is composed of ATPase enzymes

which hydrolyze one ATP / cycle, the $\Delta G^o \sim 13\ k_BT$ (50) for a full hydrolysis cycle (*E-T-D-E*). This places the following strong constraint on the rate constants:

$$\sum \Delta G^o_{ij} = \sum k_B T \ ln(k_{ij}^o / k_{ji}^o) \approx 13\ k_B T$$

The following list of additional constraints was used to tune the rate constants in the same manner as was done in Ref. (50) but with added constraints incorporated to take into account additional experimental data that was not available at the time Ref. (50) was published. As mentioned above, because my model only incorporates chemical transitions, to ensure that my rate constants produced similar behavior as those described in Ref. (50) the ratios k_{ij}/k_{ji} were tuned to produce roughly the same free energy reaction diagram as in Ref. (50) at experimental conditions ([ATP] = 250μM, [ADP] = 5 μM, and [Pi] = 5 μM) while still meeting the requirements of detailed balance.

i. The ATP binding constant k^o_{ET} was kept within the ranges used in Ref. (50) and those used later by the same authors in Ref. (20). This value was between 1 and 5 $\mu M^{-1}s^{-1}$. This value was also tuned simultaneously with the ADP release rate to match the experimentally determined Michaelis constant ($K_m \approx 25$ μM).

ii. As described in Ref. (20), ADP release events are rate limiting even at saturating [ATP], therefore k^o_{DE} was tuned to match the experimental V_{max} of ~120-130 bp/s. The ADP binding rate was kept at a similar order of magnitude to that of ATP binding since the two nucleotides are similar and ADP acts as a competitive inhibitor of ATP.

iii. The value of n_{min} (inverse of the randomness = the ratio of the squared mean of the dwell times to their variance) at saturating ATP is ~ 4 meaning that all 5 subunits do not have the same ADP release rate. Here, as was done in Ref. (20), the ADP release rate of

the special subunit was set to be 10-20 times faster than the other 4 subunits, with its reverse rate of ADP binding being accelerated by the same factor as to maintain the ΔG.

iv. The value of n_{min} at limiting [ATP] ~ 2, therefore it was necessary to set one of the ATP binding constants, that of the n_{min} must remain roughly constant across all [ADP], even those as large as [ADP]/[ATP] = 6 at [ATP] = 250 μM. The experimental data does show a slight drop in n_{min} upon closer inspection however and I found that this was necessary to also reproduce the n_{min} vs. [ATP] relationship while still reproducing the correct velocity vs. [ATP] relationship, particularly the K_m value.

vi. The relationship between the inverse velocity and [ADP]/[ATP] must be linear. This constraint insures that the ADP release and ATP binding events are tightly coupled such that only 1 subunit is in the apo (E) state at any given time. Meeting this constraint requires the introduction of certain acceleration factors as described in Ref. (50). One of which, f^{acc}_{DE}, accelerates the dissociation of ADP upon binding of ATP to a neighboring site. This acceleration factor is applied to the respective reverse transitions as well as to maintain the ΔG, thus only influencing the rates. Two additional acceleration factors were incorporated into the model as described in Ref. (50) which are f^{acc}_{TE} and f^{acc}_{DE} which were both set to 0.5 to mimic tight binding nucleotide states. These acceleration factors apply only to the designated transitions and not their reverse transitions.

vii. As described in Ref. (49), the velocity vs [ATP] relationship must fit to a general Hill equation with a Hill coefficient of ~1. This requirement comes out naturally from a system that obeys constraint ***vii***.

viii. Because the potential was disregarded, the entire force velocity relationship had to be incorporated into a force depended k_{TD}. The value of this constant was constrained to

Table 3.1. Simulation parameters.

Parameter	Value
k^{o}_{ET}	3 $\mu M^{-1}s^{-1}$
k^{o}_{TE}	7.5 s^{-1}
k^{o}_{TD}	8 s^{-1}
k^{o}_{DT}	6.1 x 10^{-11} $\mu M^{-1}s^{-1}$
k^{o}_{DE}	12 s^{-1}
k^{o}_{ED}	0.1 $\mu M^{-1}s^{-1}$
f^{acc}_{DE}	13
f^{acc}_{TD}	1000
f^{acc}_{TE}	0.5
f^{acc}_{DE}	0.5
$f^{acc}_{DE(SS)}$	5
$f^{acc}_{ET(SS)}$	0.25
$f^{acc}_{TD(SS)}$	1000

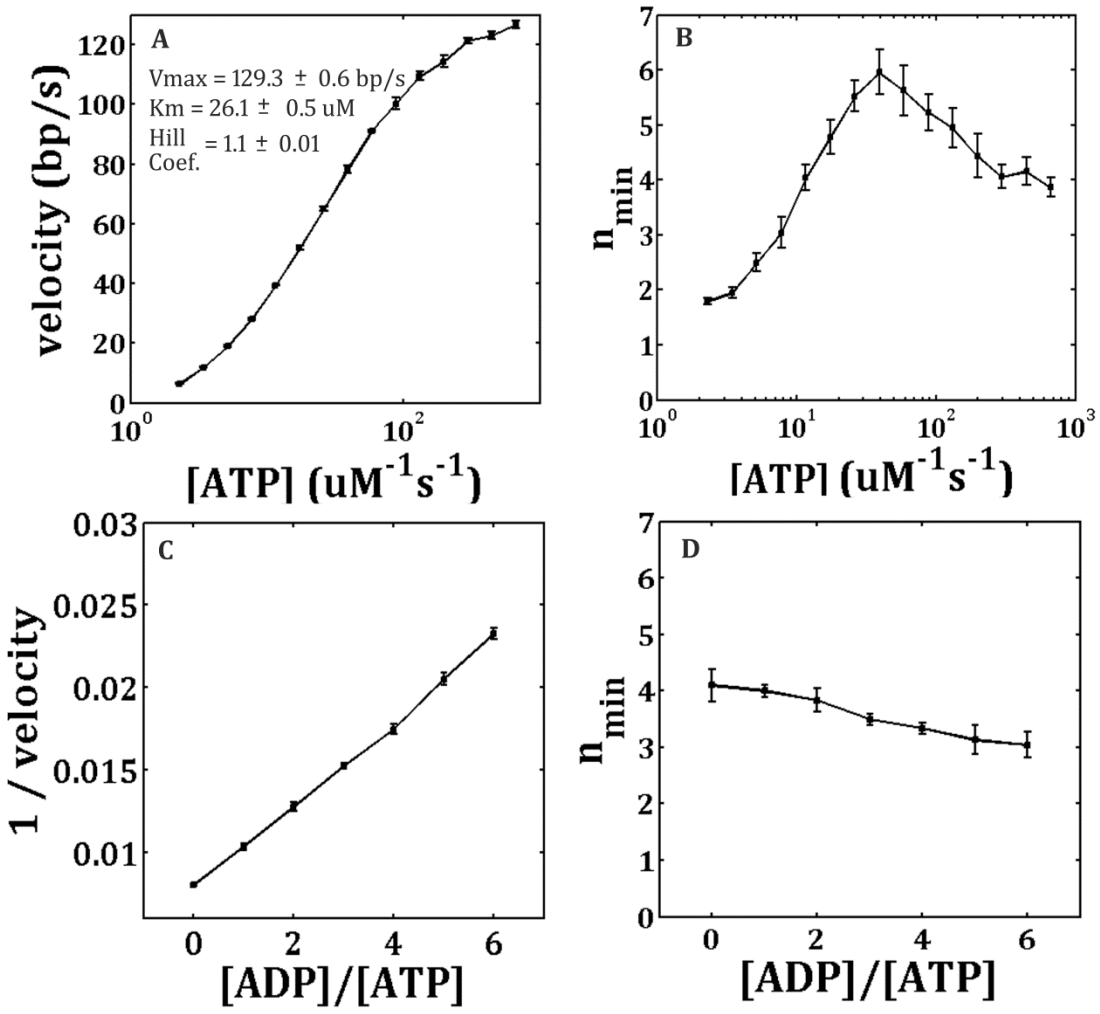

Figure 3.2. The model reproduces experimental results at low filling and low force. **(A)** Velocity vs. ATP concentration with best fit values for the parameters V_{max}, K_m, and the Hill coefficient obtained from fitting the data to the general Hill equation $v = Vmax \times [ATP]^n/(K_m^n + [ATP]^n)$. **(B)** n_{min} vs ATP concentration. n_{min} = 1/randomness parameter = squared mean over the variance in the dwell time). **(C)** inverse velocity vs. the ratio of ADP to ATP concentration ([ATP] = 250 μM) **(D)** n_{min} vs. the ratio of ADP to ATP concentration. All error bars are the standard deviation of 5 repeated simulation runs, each lasting 100s.

match the measured burst duration vs. force relationship described in Ref. (26) while k_{DT} was tuned to produce a similar ΔG_{TD} under experimental conditions (as reported in Ref. (50), here set to between 20 and 30 k_BT.

ix. In this model, as done in Refs. (20,50), the special subunit is constrained to be the one that initiates the burst and dwell phases by being the first to hydrolyze ATP and release ADP respectively. Acceleration factors are applied to the special subunit, $f^{acc}_{DE(SS),}$ $f^{acc}_{ET(SS),}$ and $f^{acc}_{TD(SS),}$ which modify the rate constants of the respective transitions and their reverse transitions.

x. A constraint not considered in Refs. (20,26,50) but which is crucial for our purposes is that the inverse of the ATP dissociation rate at low filling must be roughly 2s as was observed experimentally for the dissociation of γS-ATP from the motor in both Ref. (20,49) and in our results presented here. This dissociation rate must take into account both the standard condition dissociation rate and the effects of the various acceleration factors that influence this transition. In addition, the most recent experimental evidence described in Ref. (20) suggests that the subunit that binds γS-ATP takes on the identity of the special subunit and thus the 2s dissociation time must also take into account the additional acceleration factors applied to the special subunit. Finally, k_{TE} was also tuned simultaneously with ΔG_{ET} to produce a similar value as reported in Ref. (50), here it was set to ~5 k_BT.

The main purpose in creating this model is to explore the relationship between the observed allosteric changes in velocity with filling and the various nucleotide-motor interaction rates. However, for the results at different filling levels to be meaningful it is

important that the model reproduce all the available experimental data gathered at low procapsid filling where the allosteric effects of DNA filling are negligible. Plotted in Fig. 3.2A-D are velocity (V_{max} vs [ATP], n_{min} vs [ATP], velocity^{-1} vs the ratio of [ADP]/[ATP], and n_{min} vs the ratio of [ADP]/[ATP] respectively. Plotted in the inset of Fig 3.2A are the best fit parameters to the general Hill equation which match very closely to those published in Ref. (49). These four plots reproduce the primary features of the experimental results and their corresponding plots can be found in Refs. (20,26,49).

C. Results

1. Motor restart times after γS-ATP induced stalls depends strongly on filling.

We use optical tweezers to directly measure the packaging of single DNA molecules into single phage phi29 proheads using techniques modified from those we described previously (11, 13, 16, 23). In brief, prohead-motor complexes are attached to one microsphere and DNA molecules are attached to a second microsphere. When a DNA molecule is brought into contact with the motor in the presence of ATP packaging initiates and DNA is translocated into the prohead (Fig. 3.3a). We continuously track the length of DNA packaged vs. time by using a feedback control system to apply a constant force of 5 pN, which is small compared with the maximum force the motor can exert (>60 pN).

The most obvious way that DNA packaged inside the prohead can influence the motor function is through forces resisting DNA translocation which directly load the

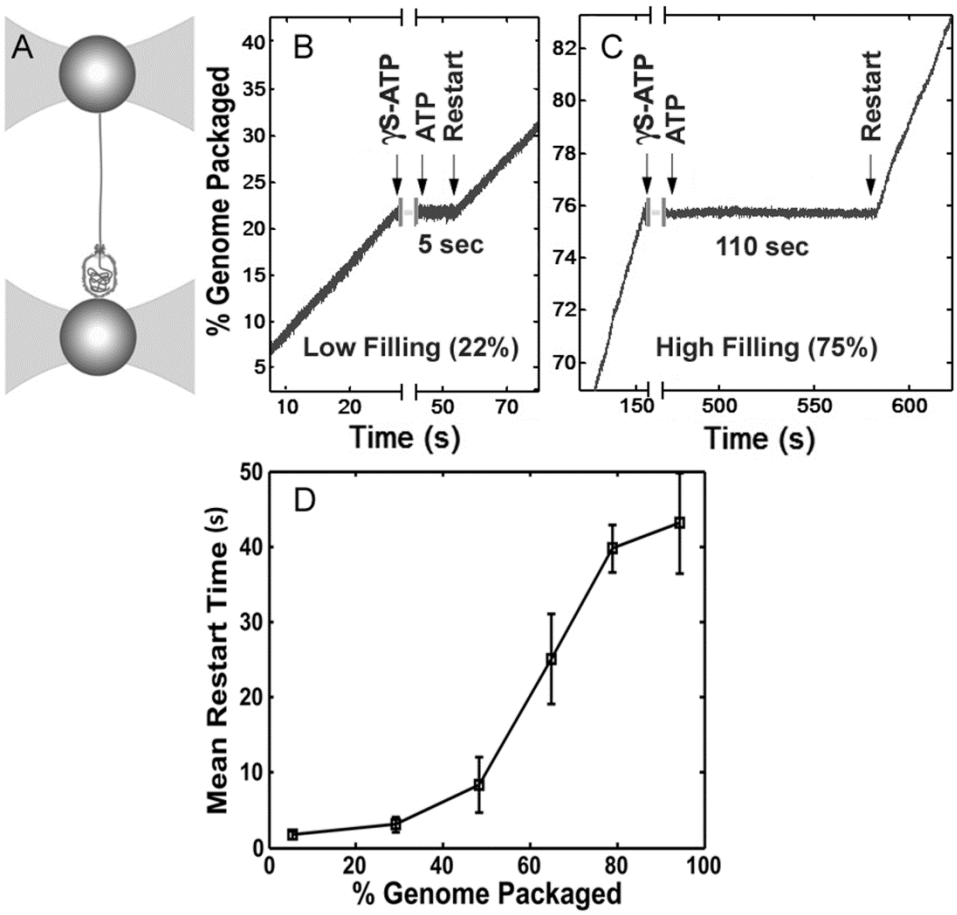

Figure 3.3. Nucleotide exchange experiments. (a) A schematic illustration of the experimental setup. A prohead-motor complex is attached to one microsphere and held in one optical trap (left) and a single DNA molecule is attached by one end to a second microsphere and its other end is packaged into the prohead**. (b-c)** Examples of nucleotide exchange experiment. The motor is stalled by addition of γS-ATP and then ATP is reintroduced and the motor is observed to restart after a delay ("restart time"). **(b)** An example of a measurement at low filling (22% genome packaged) showing a short restart time of 5 s. **(c)** An example of a measurement at high filling (75%) showing a very long restart time of 110 s. **(d).** Mean time to restart following nucleotide exchange**.** Dependence of mean restart time following exchange from γS-ATP to ATP on prohead filling (n=304 packaging events). Error bars indicate standard error in the mean.

motor, which we call “internal force” (11, 12, 18) (Fig. 3.1). These forces are expected to arise because confinement of the DNA is an energetically unfavorable process (6-10). Such internal force exerts a load on the part of the motor that grips and translocates the DNA through the portal channel and slows the motor by reducing any force-dependent rate constants in the mechanochemical cycle. In standard theoretical analyses the presence of a resisting load force Fload during a DNA translocation step of size Δx increases the mechanical work energy by an amount $F_{\text{load}}\Delta x$, which increases reaction energy barriers (30, 31). To probe the motor's response we can artificially apply a load force by applying tension to the unpackaged DNA tether (Fig. 3.1). The measured velocity v has been shown to decrease with increasing applied force Fload in accord with the formula $v = 1/(a + b\cdot\exp(c\cdot\text{Fload}))$ predicted by Chemla et al., where a, b, and c are constants related to kinetic model parameters described in Ref. 12. The motor also slows progressively as the prohead fills with DNA (11, 13, 16). Under an assumption that load force was the only factor slowing the motor, the above relationship was used to infer the magnitude of the internal force as the prohead filled (11, 16). Surprisingly, however, we present evidence here that load force is not the only factor influencing the motor function. We show that as the prohead fills, the building density of DNA has an additional effect on the motor that is distinct from the effect of load force and contributes significantly to the change in motor dynamics at high fillings.

Our first finding demonstrating this effect comes from measurements in which we stalled the motor with a non-hydrolyzable ATP analog (γS-ATP) and restarted it by reintroducing ATP. This was done by moving the packaging complex in front of a capillary dispensing γS-ATP and then moving it back into the main flow chamber

containing ATP. In this manner we achieved exchange back to ATP in <1 s. Strikingly, we find that the time it takes the motor to restart following this nucleotide exchange is strongly dependent on prohead filling. At low prohead filling the motor restarts rapidly, within a few seconds (Fig. 3.3b), but at high filling the restart time can increase to longer than 1 minute (Fig. 3.3c). The average restart time measured for an ensemble of experiments increases continuously with increasing prohead filling (Fig. 3.3d). This increase is not attributable to increasing load force because it has been previously shown that the dissociation rate of γS-ATP measured at low filling is independent of applied force (12). Our present finding therefore implies an indirect effect of prohead filling on motor-ATP interactions.

2. The frequency and duration of intrinsic motor pauses increases with filling but not force

Our second finding demonstrating this effect comes from detailed studies of pausing in DNA translocation. In measurements with low load (5 pN) we observe short pauses of typically ~1-10 seconds in DNA translocation that occur with a frequency that increases strongly with increasing filling (Fig. 3.4a), also observed in earlier studies (11, 23, 26). We present additional data here showing that pausing, measured at low prohead filling, is not significantly induced by increasing load (Fig. 3.4b). Thus, the observed increase in pausing with increasing filling cannot be attributed to buildup of force resisting DNA translocation and, rather, must be attributed to an independent effect of prohead filling on motor function.

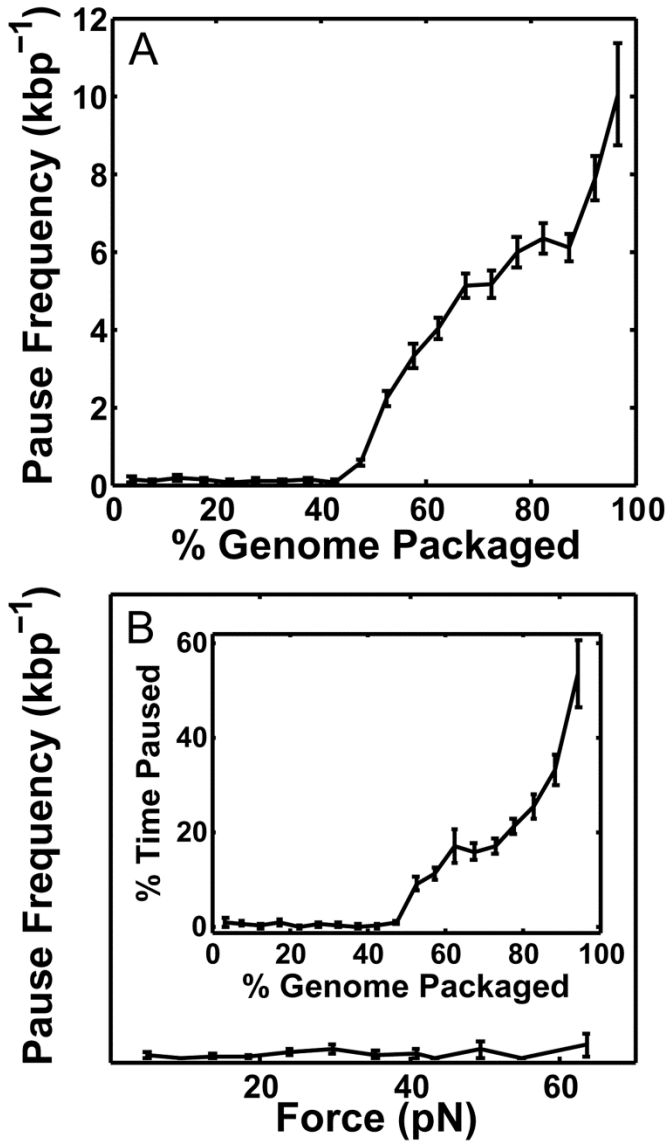

Figure 3.4. Analysis of pauses in motor translocation. (a) Mean frequency of pauses (number detected per kbp packaged) vs. prohead filling (n=45). **(b)** Mean frequency of pauses vs. applied force (n=130). Inset shows the % time spent paused. All error bars indicate standard error in the mean.

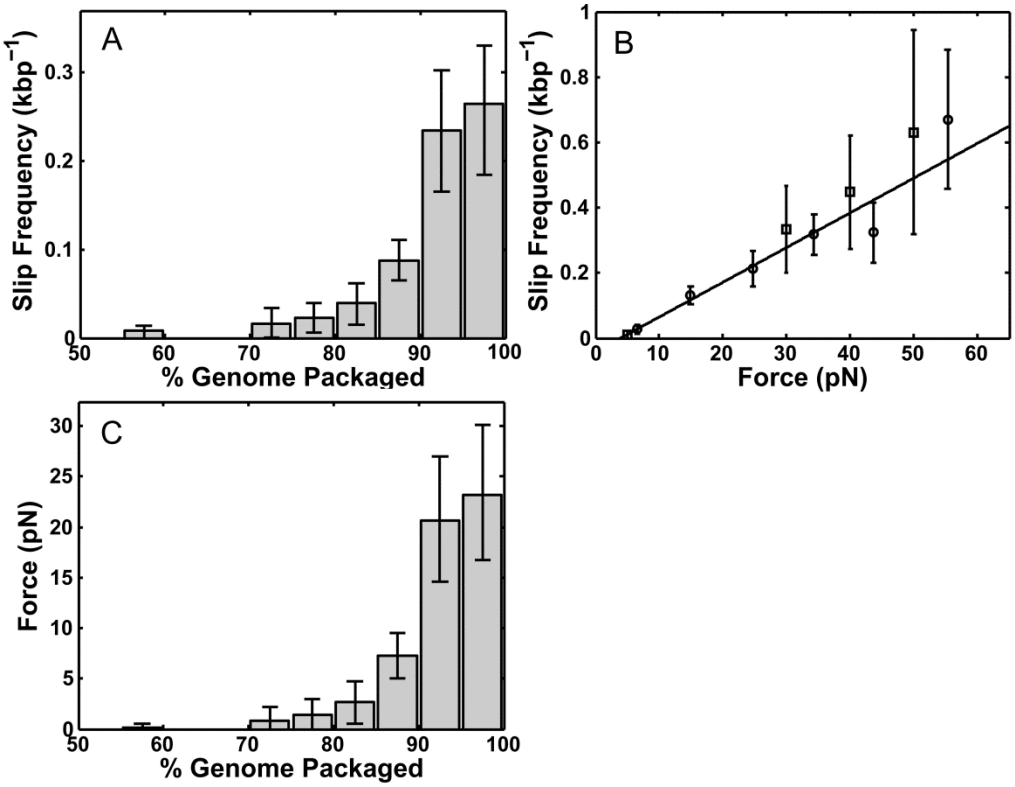

Figure 3.5. Analysis of motor slipping. (a) Mean frequency of slips (number detected per kbp packaged) vs. prohead filling measured with a 5 pN force clamp (n=320 packaging events). (b) Mean frequency of slips vs. applied force measured at low filling (<20%) in both force clamp mode (where force is held constant at different preset values; circles, n=190) and fixed trap positions mode (where force is allowed to build as packaging proceeds; squares, n=130). The solid line is a linear fit to the data points. (c) Force resisting packaging vs. prohead filling inferred from plots a&b. All error bars indicate standard error in the mean

3. The frequency of motor slipping increase with applied load but not with filling

Our third finding demonstrating this effect comes from studies of motor slipping. Slips were defined as events in which a length of DNA suddenly came backwards out of the prohead, typically ~30-150 bp. In sharp contrast to the trend observed with pausing, the frequency of slipping increases both with increasing filling (Fig. 3.5a) and with increasing applied load (Fig. 3.5b). We interpret these findings as indicating that slipping occurs when the motor loses grip on the DNA and that theprobability of slipping increases with increasing load. In this case, the buildup of load force can be inferred by relating the frequency of slipping vs. load force, measured at low filling, to the frequency of slipping vs. filling (Fig. 3.5c). The inferred internal force is very low (<1 pN) until ~70% filling, where it then begins to builds rapidly and reaches a maximum of ~23 ± 7 pN at the end of packaging.

In earlier analyses, we inferred internal force under the seemingly reasonable assumption that the decrease in motor velocity with filling is completely due to this force loading the motor (11, 13 and 16). However, the magnitude of the internal force deduced under that assumption is several-fold higher than that inferred from our present measurements of slipping frequency (Fig. 3.5B). Most notably, the motor velocity (i.e., the packaging rate not including pauses and slips) decreases by ~50% going from 0% to 70% prohead filling (Fig. 3.6A), but the measurements of slipping suggest that there is very little internal force (<1 pN) up to this point. Based on the measured velocity versus load force relationship (Fig. 3.6B), 1 pN of internal force would only cause a ~2%

reduction in velocity, which cannot explain the measured ~50% velocity decrease going from 0% to 70% filling. Thus, these findings further demonstrate that much of the slowing of the motor is not caused by load force and again must be attributed to an indirect effect of the packaged DNA on motor function.

D. Discussion

1. An unconventional type of allosteric regulation

We refer to the reported slowing of the motor with prohead filling due to modulation of motor-ATP interactions as allosteric regulation in analogy to the classical phenomenon wherein an enzyme's activity at one site is regulated by the binding of an effector molecule at a second site. Here, the motor's DNA translocase activity, which is coupled to the ATP hydrolysis cycle, is allosterically regulated by the presence of increasing amounts of DNA packaged inside the prohead. This allosteric signal negatively regulates the packaging rate by both reducing the motor's translocation speed and increasing the frequency of pauses. This regulation likely helps to mitigate the formation of non-equilibrium DNA conformations that we have demonstrated can cause stalling and slipping of the motor (23, 32).

We note that this regulation is unlike typical allosteric regulation in two ways. First, the prohead filling sensor is non-specific in the sense that it does not appear to involve binding of a specific DNA sequence to a complementary binding site. Studies using several different DNA substrates observe motor slowing independent of the sequence being packaged (11, 13, 16, 23, 32). Rather the motor function is modulated by

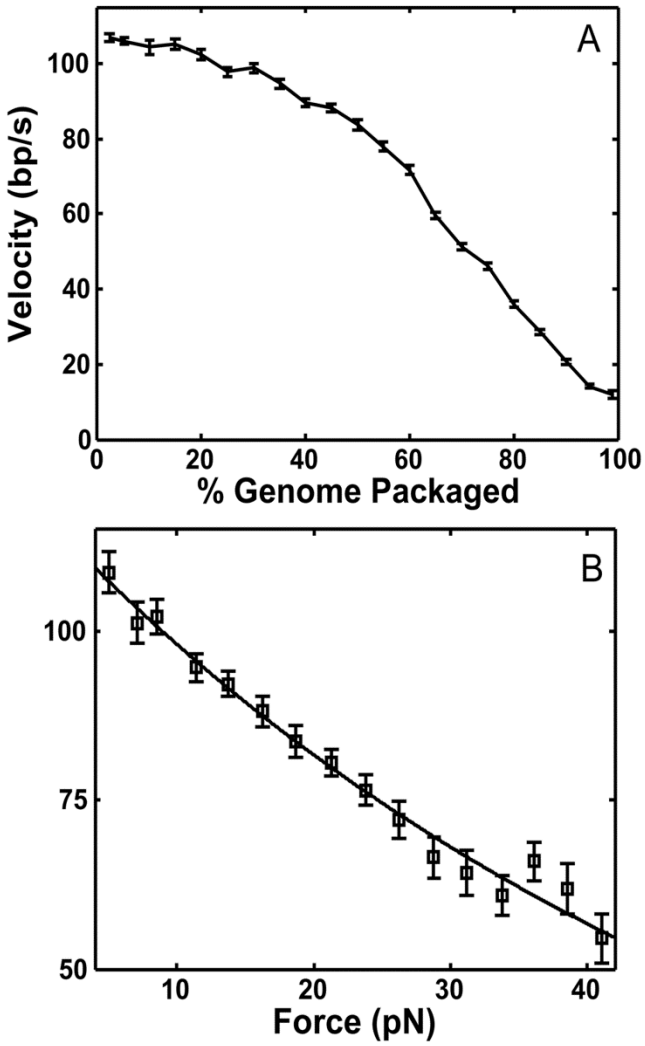

Figure 3.6. Motor velocity measurements. (a) Mean velocity vs. prohead filling (n=45). (b) Mean velocity vs. applied force (n=74). All error bars indicate standard error in the mean.

an increasing density of confined DNA, presumably through non-specific interactions with the portal and/or prohead wall. Second, whereas binding of an effector molecule typically causes a discrete change in enzyme activity, here the velocity of the motor complex decreases continuously with increasing length of DNA packaged. Since our experiments directly measure the rates of single motor complexes, it is clear that this continuous change is of the activity of individual motors and not simply due shifting sub-populations of complexes having two distinct activity levels (e.g., with effector bound vs. unbound).

2. Structural basis for the allosteric effect

Structural studies based on cryo-electron microscopy show that the portal channel through which the DNA is translocated extends from the interior of the prohead to the exterior where the motor protein is attached via the intervening pRNA (Fig. 3.1) (25, 33, 34). The force resisting DNA packaging is directly transmitted to the motor via its contacts with the section of DNA threaded through the channel (Fig. 3.7a). However it is quite clear that the section of DNA already packaged inside the prohead does not directly contact the motor protein and therefore cannot directly affect its operation. The packaged DNA only touches the inner wall of the prohead and a portion of the portal channel that extends into the prohead interior (25, 33, 34). Our results therefore imply that the packaged DNA must interact with the motor protein via a long distance allosteric signal (Fig. 3.7b). This signal must be transmitted ~100Å from the interior of the prohead to the motor on the exterior via the intervening prohead shell and/or portal protein and pRNA.

Cryo-electron microscopy studies (Cryo-EM) of several different phages including phi29 show that the packaged DNA is in contact with the portion of the portal

channel exposed to the interior (25, 34-39). Two particularly striking observations are: (i) a ring of DNA appears to wrap around the portal, appearing to "squeeze" it, and (ii) the portal adopts a different conformation when incorporated in the head than is observed for isolated portals (37, 38). Because the portal was only imaged at one filling level (fully packaged) it is unclear if the alternate conformation that putatively triggers termination represents one conformation of a two-state system or a single point in a continuum of conformational states. Our data supports the later scenario for phi29 motor regulation since we observe a continuous decrease in velocity for individual complexes and large heterogeneity among an ensemble of complexes (23). Mutant studies also indicate that residue changes in the portal protein can affect the length of DNA packaged (40). Unlike phi29, P22 packages by a "headful" mechanism in which the motor must excise a unit-length genome from a concatenated DNA substrate (3, 4, 37). The motor is triggered to terminate packaging and cleave the DNA after an appropriate genome length has been packaged. It was proposed that the conformational change observed in the P22 portal may be the signal that triggers the termination (37). CryoEM and molecular dynamics studies of phage epsilon15 also revealed a well-resolved ring of averaged density located inside the narrow groove at the base of the portal (36, 41). In simulations this groove section often consists of variable arrangement of two or more independent DNA segments (23). Cryo-EM studies of phi29 virions also reveal a ring of DNA in contact with the portal, although it is touching the "top" of the portal rather than being wrapped around it (34). Although phi29 does not package by a headful mechanism, an analogous conformational change in its portal, induced by contact with the packaged DNA, could communicate the allosteric regulatory signal to the motor protein.

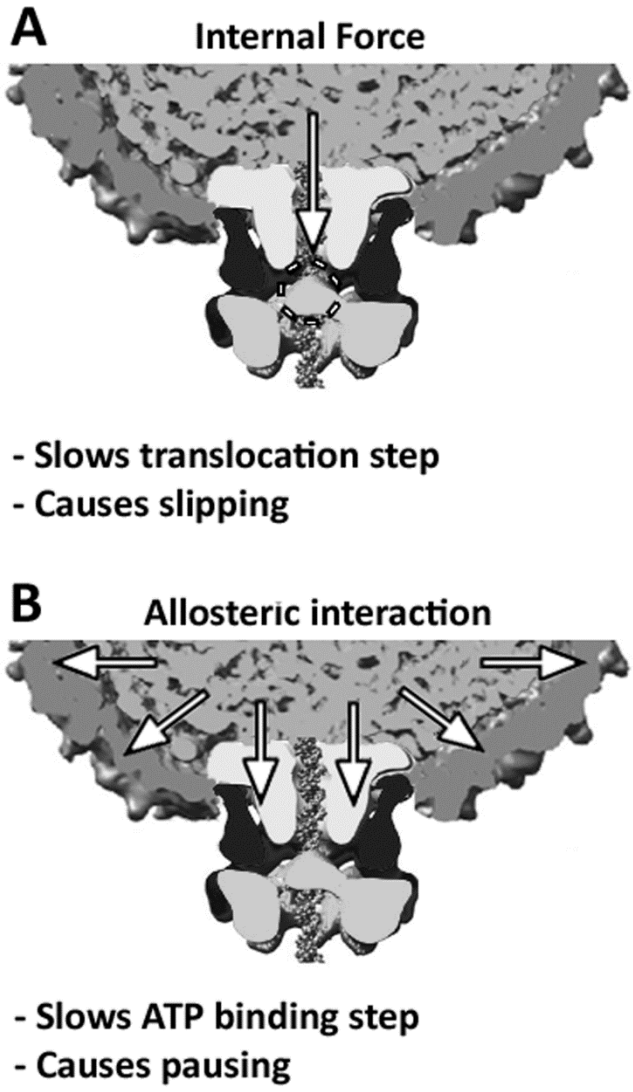

Figure 3.7. Two different mechanisms of regulation of the phi29 motor. (a) Forces acting directly on the section of DNA entering through the portal exert a direct load on the portion of the motor that grips and translocates the DNA (dashed circle). (b) DNA packaged inside the prohead interacts with the inner wall of the prohead and portion of the portal protein which protrudes into the interior. This interaction allosterically regulates the motor protein attached to the exterior portion of the portal, in a manner distinct from direct load. Images constructed as in Fig. 3.1.

3. Distinction between the effects of load and allosteric regulation

While we have distinguished motor slowing due to internal force that directly loads the motor from that due to allosteric regulation, the latter could still be caused by conformational changes induced by the buildup of internal forces. As illustrated in the schematic diagram in Fig. 3.7a and b, the force per unit area (pressure) exerted by the packaged DNA on the inner surface of the prohead wall and portal ring is presumably similar or equal, on average, to that resisting translocation of DNA by the motor through the portal channel. However, our findings show that the onset of the slowing due to the allosteric mechanism occurs at a much lower filling than slowing due to force directly loading the motor. If the allosteric mechanism is indeed triggered by internal force it must be much more sensitive to the magnitude of the force (i.e., triggered by lower forces than are needed to significantly slow the motor via load). Specifically, as discussed below, analysis of motor slipping reveals that the allosteric effect begins to significantly slow the motor well before any changes in load-dependent behavior are detected (i.e. slipping). Although we could not detect any internal force below ~70% filling it is likely that a small internal force (e.g., <1 pN, below that our slipping analysis can detect) does build up, as expected theoretically. Such low force would not significantly slow the motor via load (Fig. 3.6a), but could be more than sufficient to trigger motor slowing via the allosteric mechanism.

4. Effect on motor-ATP interactions

Our finding that motor restart time following exchange from γS-ATP to ATP increases dramatically with prohead filling shows that the motor-ATP interaction is

affected. In principle, either a decrease in ATP binding rate or an increase in ATP dissociation rate would slow the motor (12), but our measurements rule out the latter possibility, as follows. Fig. 3.4.2d shows that the restart time at 70% filling is ~30 seconds, but at this filling the motor velocity during packaging is ~50 bp/s, which implies that one ATP is being hydrolyzed every 0.04 s (since ~2 bp are packaged per ATP) (12). Thus, ATP binding, hydrolysis, DNA translocation, and ADP and phosphate release must all happen very rapidly in 0.04 s. The 30 s restart time we measure must therefore be attributed to slow dissociation of γS-ATP. Our measurements thus imply that the γS-ATP dissociation rate decreases with increasing prohead filling. Since γS-ATP has been shown to mimic ATP in its binding kinetics (12), this implies that if ATP had the opportunity to dissociate (as opposed to being rapidly hydrolyzed) its rate of dissociation would decrease with increasing prohead filling. A decreased dissociation rate, however, would increase motor velocity, and therefore cannot explain the observed reduction with filling. Therefore, we attribute the reduction in motor velocity to a decrease in the ATP binding rate.

A decrease in ATP binding rate could occur due to either to weakening of the motor-ATP interaction or to occlusion of the ATP binding pocket. Our evidence that the rate of ATP dissociation decreases with increasing filling suggests that it is due to occlusion. Such occlusion could be caused by a conformational change in the motor protein that affects the ATP binding pocket or conformational changes in the prohead, portal, and/or pRNA components that result in steric hindrance of the entry of ATP into the binding pocket.

5. Contributions of load vs. allosteric regulation to motor slowing

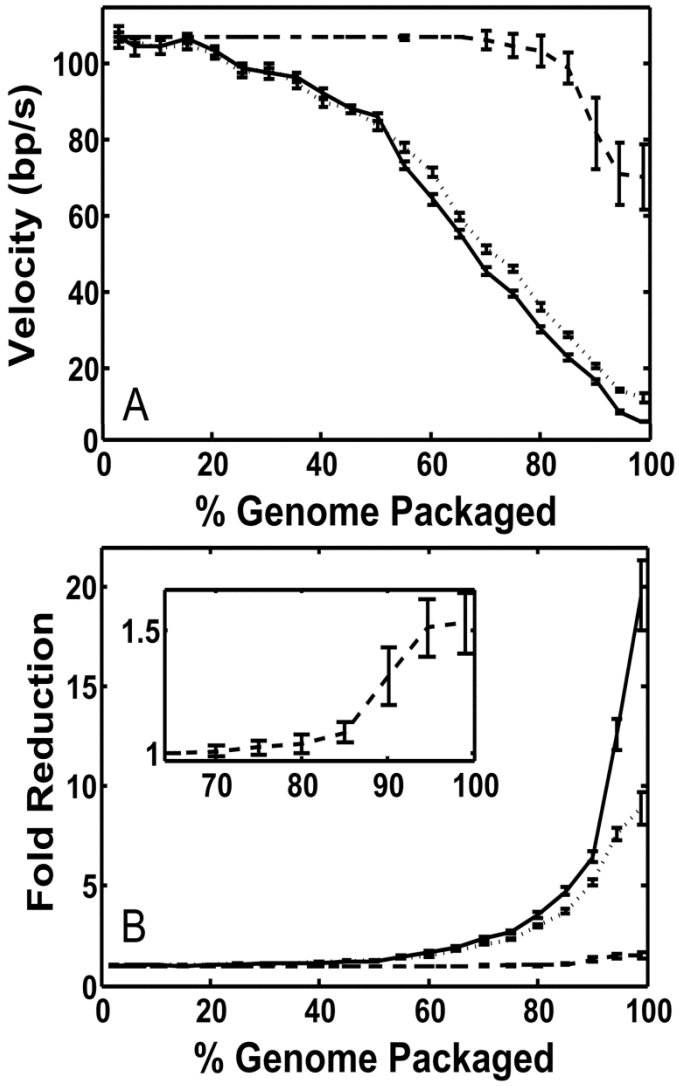

Figure 3.8. Factors influencing reduction in motor velocity. (a) Measured mean packaging rate (solid line) and measured mean motor velocity (rate not including pauses and slips, dotted line) vs. filling compared with the velocity that would be expected if the force plotted in Fig.

The magnitude of internal forces implied by our measurements of motor slipping (Fig. 3.5c) are significantly lower than those estimated previously under the assumption that internal force was the only factor slowing the motor (11, 13, 16). This discrepancy is explained by our present finding that prohead filling has an independent allosteric effect on motor function. Our measurements of motor slipping suggest that the internal force is quite low (<1 pN) until ~70% filling, after which it rises sharply. The ~50% decrease in motor velocity going from 0 to 70% filling is therefore almost entirely attributable to allosteric regulation.

In Fig. 3.8a, we compare the measured dependence of motor velocity vs. filling to that which would be expected due to the buildup of internal force loading the motor alone. The change in velocity was inferred from relating the inferred internal force-filling relationship in Fig. 3.5c to the measured force-velocity relationship in Fig. 3.6b. This comparison shows that allosteric regulation begins slowing the motor significantly at ~20% filling, whereas slowing due to the buildup of internal force starts much later, at ~70% filling. We also plot for comparison the overall mean packaging rate, which includes the effect of motor pauses and slips (Fig. 3.8a). At low filling (<50%) pauses and slips cause negligible percent change but pauses steadily increase in importance at high filling (see also Fig. 3.4b inset).

Overall, the allosteric mechanism, which both slows the motor velocity and causes pausing, has a much larger effect on packaging kinetics than internal force. Comparisons of the ratio of the initial velocity (Vmax) to the expected velocity if force alone slowed the motor, and to the ratio of Vmax to the measured velocity, are plotted in Fig. 3.8b. This shows that internal force alone is predicted to have only a minor impact

on the overall velocity change, accounting for a ~1.5-fold reduction from the initial value, whereas the actual reduction reaches ~8-fold near the end of packaging. Thus, the allosteric interaction ultimately slows the motor velocity by an additional ~5 fold. The reduction in overall packaging rate, which includes the effect of pauses, reaches ~20-fold near the end of packaging. Thus, allosterically-induced pauses ultimately slow packaging by an additional ~2.5-fold.

6. Force resisting DNA confinement and comparisons with theories

Our findings shed new light on discrepancies between our earlier higher estimates of forces resisting packaging (internal force) and theoretical predictions (7-9, 13, 16, 42-44). Our present measurements of slipping suggest very little buildup of force from 0 to 70% filling, followed by a rise to ~23 pN near the end of packaging. This trend is in closer accord with theoretical predictions based on continuum mechanics models and measurements of forces driving DNA ejection (45). Specifically, Tzlil et al. calculate an initially low rise and maximum force of ~25 pN based on a model assuming an inverse-spool conformation of DNA and interaction potential derived from measurements of DNA condensation by osmotic pressure (7). Caveats in this comparison are that their study modeled phage lambda, which has a different shape and genome length and slightly higher packing density, considered slightly higher ionic screening, and did not consider non-equilibrium effects (23, 46). Calculations by Purohit et al. using a similar model, but specifically considering the phi29 prohead size, shape, and packing density, also predict a similar shape of the force vs. filling curve, though they do not make absolute predictions of the forces independent of previously reported experimental estimates (8).

Packaging has also been modeled using coarse-grained molecular dynamics simulations. Forrey and Muthukumar calculated a maximum resisting force of ~40 pN (9), which is higher than we find here, though again did not specifically model the phi29 prohead dimensions. Another caveat in this comparison is that DNA packaging was simulated at an initial rate ~10^5 *x* faster than the experimental rate due computational constraints, which could cause larger deviations from equilibrium and higher forces. Petrov and Harvey also conducted molecular dynamics simulations using a DNA interaction potential derived from available osmotic pressure data for similar ionic conditions. They calculated resisting forces rising to ~60 pN (44). Again however, the simulated packaging was much faster than the natural speed (1 nm steps every 10 ns, although the authors point out that this timescale does not translate to experimentally measured time due the use of a coarse grained model for DNA). Again, faster packaging could explain larger deviations from equilibrium and higher forces. Specifically, the finding of higher forces in these simulations may be due to an inability of the simulations to model the very slow DNA relaxation dynamics which we have shown to occur on >10 minute timescales (23).

7. Regulation responds to changes in both length and conformation of packaged DNA

We have shown that packaging is not a quasistatic process because at high filling the DNA forms non-equilibrium conformations that relax on a timescale longer than the packaging reaction (23). When packaging was stalled at ~75% filling for ~12 minutes (on average), to allow the DNA to relax, the average motor velocity increased by ~23% after

restarting. Notably, this change occurred with no change in prohead filling, indicating that this effect must be caused solely by a change in the conformation of the packaged DNA. At 75% filling the internal force implied by our measurements of slipping is <2 pN. According to the measured force-velocity relationship (Fig. 3.6b), at 75% filling the complete relaxation of 2 pN of force would only cause a ~4% change in velocity, so the observed velocity increase following DNA relaxation cannot be attributed to the relaxation of internal force alone. Thus, this acceleration must mostly be attributed to modulation of motor activity via the allosteric regulatory mechanism.

We also found that the frequency and duration of pauses decreased dramatically after the DNA was allowed to relax (23). Since we have shown here that pausing is not significantly induced by load force, the change in pausing dynamics after DNA relaxation must therefore be attributed to changes in the packaged DNA conformation that alter the interaction(s) responsible for the allosteric effect. Remarkably, these findings on both motor velocity and pausing imply that the allosteric sensor we have described responds not only to the prohead filling, but also to the conformation of the packaged DNA.

Earlier studies by our lab (13) also showed that the decrease in velocity with filling is dependent on ionic conditions which can change the packaged DNA conformation (47, 48). In conditions where the DNA-DNA interaction is purely repulsive, higher screening (with Mg2+, cobalt hexamine3+, or spermidine3+) results in a later onset of motor slowing, consistent with decreased internal pressure causing decreased allosteric regulation. In addition, we recently found that high levels of spermidine, sufficient to induce DNA condensation in solution (changing the DNA-DNA interaction to partly attractive) causes significant slowing of the motor as well as more

frequent and longer pauses even at low filling levels (<50%) (32). While this finding is contrary to theoretical studies that predicted reduced forces resisting DNA confinement, our interpretation is that attractive interactions exacerbate the formation of highly non-equilibrium DNA conformations that result in higher resistance forces and/or greater allosteric slowing (34).

8. Relationship with motor stepping kinetics

Previously it has been shown that packaging occurs in rapid bursts of four 2.5 bp steps separated by dwells (18). At low filling the duration of the bursts is independent of ATP concentration but increases with increasing applied force, whereas the duration of dwells depends on ATP concentration but not applied force. A study published very recently by S. Liu et al. reported that the duration of the dwells also increases with increasing prohead filling (26). The conclusions we reach here are consistent with these findings. First, the reported increase in the duration of dwells with increasing prohead filling causes a load-independent decrease the motor velocity, consistent with our findings. Second, our measurements of motor restart time following nucleotide exchange imply force independent changes in motor-ATP interactions and suggest that motor slowing is due to slowed ATP binding. Previous measurements showed that motor velocity vs. [ATP] follows Michaelis-Menten kinetics (12). Liu et al. extended these measurements to show that the maximum velocity (Vmax), Michaelis constant (KM), and their ratio (Vmax/KM) decrease with increasing filling, suggesting that filling slows ATP binding, consistent with our conclusion. Third, our measurements of slipping frequency vs. filling and vs. force suggest internal force remains low (<1 pN) until ~70% filling and then rises steeply to ~23 pN near the end of packaging. Through a different method, Liu

et al. infer internal force by relating the dependence of the duration of bursts of translocation steps on filling to their dependence on applied force, yielding a force which rises in a similar manner to a maximum value of ~20 pN (26). That these two different methods of determining internal force yield very similar values provides strong support for the validity of these results.

9. Monte Carlo simulations

To gain a more quantitative understanding of the relationship between the observed allosteric slowing of the motor and changes in ATP–motor interactions , I ran stochastic simulations of the phi29 packaging motor according to the procedure outlined in Ref. (50) while also updating the model to incorporate all new experimental data, particularly from Refs. (20,26,49). A detailed description of the model and the simulation procedure can be found in the methods section. My reasoning is that if I can first create a working model that reproduces all the of the data from the experiments conducted at low procapsid filling where the allosteric effect is not active then I can meaningfully explore how the different nucleotide exchange rates must change in order to reproduce the experimentally observed velocity changes. In particular, the changes in γS-ATP dissociation rates we observe with procapsid filling should scale in proportion to the changes in ATP binding rates implied by the large drop in packaging rate before the onset of significant internal forces. In Fig. 3.8B we plotted the fold change in maximum packaging rate attributed to each effect, with allosteric changes in ATP-motor interactions being responsible for all the slowing prior to ~50% procapsid filling and contributing ~5 of the total ~20 fold reduction in rate by the end of packaging. From this information we can calculate the predicted velocity-filling relationship if ATP-motor

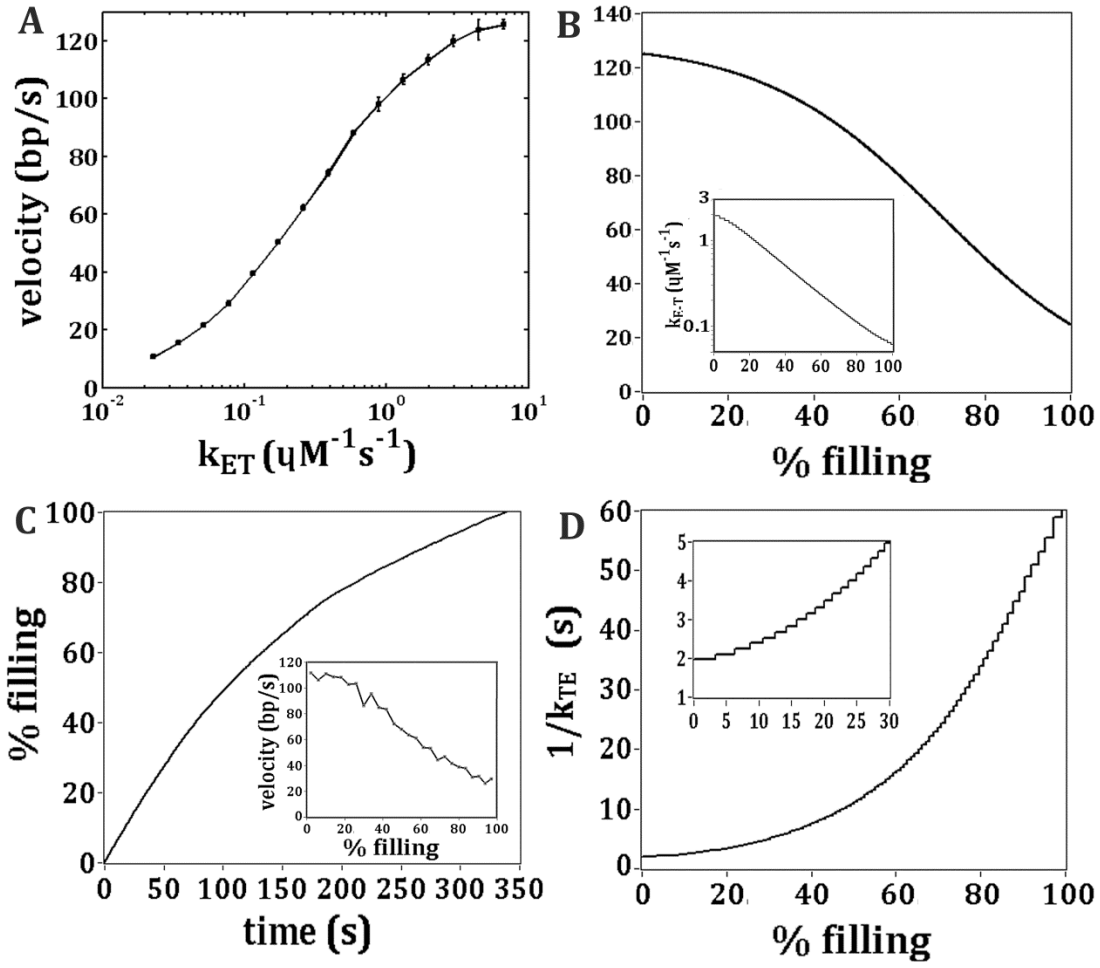

Figure 3.9. Monte Carlo simulations can predict ATP dissociation rates. **(A)** Predictions of packaging velocity across a range of ATP binding rates when the ΔG_{ET} is held constant. Error bars are standard deviation of 5 independent simulations. **(B)** Approximation of the average packaging velocity if allosteric changes in ATP binding were the only cause of slowing. Inset shows the corresponding ATP binding rates drawn from a fit of Fig. 3.8A to the general Hill equation described in Fig. 3.2 **(C)** Example of a single stochastic simulation in which the ATP binding constant was continuously tuned to match the velocity-filling curve seen in **B**. The inset is the corresponding velocity-filling data for that single trace calculated by linear fits to a 10s sliding window showing how it matches **B**. **(D)** Predicted average ATP dissociation time (from the special subunit) vs. filling corresponding to the velocity-filling relationship in **B.** The model was tuned to match the experimentally determined γS-ATP dissociation time at low filling (1-10%). For a comparison to experimental data see Fig.3.3. Inset is zoomed in to the first 30%. Stepping behavior is a result of drawing from a discretized array of k_{ET} values.

interactions alone were slowing the motor (Fig. 3.9b). This velocity-filling relationship can then be used to tune rate constants in the simulation to reproduce the observed changes in velocity (Fig. 3.98B-C). In a model where the ATP binding pocket becomes more occluded with filling it is reasonable to assume that the relative free energy difference between the ATP bound and ATP unbound states does not change, only the barrier height between them. Then, because of the requirement of detailed balance (see methods), both the forward and backwards rates must change in proportion to one another. Fig. 3.9A shows the relationship between motor velocity and the standard condition ATP-binding rate produced when the binding and unbinding rates are tuned to maintain a constant free energy difference between the bound and unbound states. In combination with the predicted velocity- filling relationship resulting from allosteric changes alone (not force or pausing, Fig. 3.9B) one can calculate how the ATP dissociation rate would scale with procapsid filling. If the slowing of the γS-ATP dissociation rate observed in our nucleotide exchange experiments is in fact related to the slowed ATP binding rates implied by the reduction in motor velocity then the predicted ATP dissociation rates should match our experiments. Plotted in Fig. 3.9D is the inverse ATP dissociation rate vs. procapsid filling, or the average residence time of an ATP molecule on a single motor subunit (assuming it isn't hydrolyzed first). Because their binding rates have been shown to be similar, this value can then be assumed to predict the length of γS-ATP induced pauses at different fillings. Indeed, it is clear that our measured motor restart times match the ATP residence times predicted from the model quite well. It should be noted the model I use here is a 3-state chemical model and does not include

and explicit ATP tight binding, however the tight binding effect was mimicked by a tight binding "acceleration factor" as described in Ref. (50) and in the methods section. Also, according to Ref. (20), upon binding γS-ATP, that subunit takes on the identity of the "special subunit," which under the current model, has a reduced ATP binding rate from the other 4 subunits which also had to be taken into account when calculating the residence times (see methods section for more details). This result provides additional support to our conclusions based on motor restart times and provides convincing evidence that the different filling effects observed by us and Liu et al are in fact the same phenomena. Additionally these results strengthen the hypothesis that the nucleotide binding pocket is becoming occluded, possibly by a "tightening" effect around the pentameric ring of gp16 monomer. This hypothesis is also supported by that fact that homology models place the ATP binding pocket of gp16 directly at the interface between adjacent subunits where it is easy to imagine such an effect occurring. When modeling the allosteric change in velocity from the fold change data I used exponential functions and thus deviations of the experimental restart times from the predicted ones at very high filling are likely do to the fact that the real relationship is not a pure exponential. Also, in the actual experiment, the DNA is undergoing non-equilibrium dynamics and relaxations from higher energy states, thus causing complex and heterogeneous changes in binding rates at high filling not accounted for in the model. DNA relaxation effects may explain the plateauing behavior seen in our restart time vs. filling data as well as the plateauing observed in other high filling data.

10. Conclusions

We have presented three different findings which clearly indicate that prohead filling has a strong and indirect effect on the function of the motor distinct from the effect of a direct load force. First, motor-ATP interactions are strongly perturbed by filling but not by load. Second, motor pausing increases sharply with increasing filling but not with load. Third, the maximum internal force resisting packaging inferred from measurements of motor slipping is several-fold lower than previous estimates based on motor velocity, which implies that much of the reduction in motor velocity is independent of load. The implication of these findings is that an allosteric signal acts to continuously reduce the packaging rate even prior to the buildup of significant internal force. This signal is propagated ~100Å from the interior of the prohead to the motor protein mounted on the exterior.

Remarkably, the allosteric sensor responds to not only the quantity of packaged DNA but also its conformation, an effect which we propose mitigates the formation of highly non-equilibrium DNA conformations which we have shown can slow and stall the motor and cause the DNA to slip out (23, 32). Specifically, when the DNA is given less time to relax towards equilibrium this mechanism slows the motor and induces pauses. Conversely, the motor speeds up and pauses less when the DNA is given more time to relax (23). Thus the motor speed appears to be tuned by this regulatory mechanism to achieve sustainably fast packaging rates dependent on filling level and DNA conformation.

All of Chapter III except sections **B.5** and **D.8**, and Figs. 3.2 and 3.8, and table 3.1, is a reprint that the dissertation author was the principal researcher and author of. The material appears in *Biophysical Journal*. (**Z. T. Berndsen,** N. Keller, D. E. Smith.

(2015). Continuous Allosteric Regulation of a Viral Packaging Motor by a Sensor that Detects the Density and Conformation of Packaged DNA, *Biophysical Journal*, 108 (2), 315-324)

E. References

1. Smith D. E. (2011) Single-molecule studies of viral DNA packaging. Curr. Opin. Virol. 1:134.

2. Chemla Y. R. and Smith D.E. (2012) Single-molecule studies of viral DNA packaging; In Viral molecular machines, Rao, V., Rossmann, M. G., editors. Springer, New York, NY. 549-584.

3. Casjens S. R. (2011) The DNA-packaging nanomotor of tailed bacteriophages. Nature Reviews Microbiology. 9:647-657.

4. Feiss M. and Rao V. B. (2012) The bacteriophage DNA packaging machine; In Viral molecular machines, Rao, V., Rossmann, M. G., editors. Springer, New York, NY. 489-509.

5. Morais M. C. (2012) The dsDNA packaging motor in bacteriophage ø29; In Viral molecular machines, Rao, V., Rossmann, M. G., editors. Springer, New York, NY. 511-547.

6. Riemer S. C. and Bloomfield V.A. (1978) Packaging of DNA in bacteriophage heads - some considerations on energetics. Biopolymers. 17:785-794.

7. Tzlil S., Kindt J.T., Gelbart W.M. & Ben-Shaul A. (2003) Forces and pressures in DNA packaging and release from viral capsids. Biophys. J. 84:1616-1627.

8. Purohit P.K., Inamdar M. M., Grayson P. D., Squires T. M., Kondev J., Phillips R. (2005) Forces during bacteriophage DNA packaging and ejection. Biophys. J. 88:851-866.

9. Forrey C. and Muthukumar M. (2006). Langevin dynamics simulations of genome packing in bacteriophage. Biophys. J. 91:25-41.

10. Harvey S.C., Petrov A.S., Devkota B. & Boz M.B. (2009) Viral assembly: A molecular modeling perspective. Phys Chem Chem Phys. 11:10553-10564.

11. Smith D.E., Tans S.J., Smith S.B., Grimes S., Anderson D. L. & Bustamante C. (2001) The bacteriophage phi29 portal motor can package DNA against a large internal force. Nature. 413:748-752.

12. Chemla Y.R., Aathavan K., Michaelis J., Grimes S., Jardine P.J., Anderson D.L., Bustamante C. (2005) Mechanism of force generation of a viral DNA packaging motor. Cell. 122:683-692.

13. Fuller D.N, Rickgauer J.P., Grimes S., Jardine P.J., Anderson D., Smith D. E (2007) Ionic effects on viral DNA packaging and portal motor function in bacteriophage phi 29. Proc. Natl. Acad. Sci. U. S. A. 104:11245-11250.

14. Fuller D.N., Raymer D.M., Rickgauer J.P., Robertson R.M., Catalano C.E., Anderson D.L., Grimes S., Smith D.E. (2007) Measurements of single DNA molecule packaging dynamics in bacteriophage lambda reveal high forces, high motor processivity, and capsid transformations. J. Mol. Biol. 373:1113-1122.

15. Fuller D.N., Raymer D.M., Kottadiel V.I., Rao V.B. & Smith D.E. (2007) Single phage T4 DNA packaging motors exhibit large force generation, high velocity, and dynamic variability. Proc. Natl. Acad. Sci. U. S. A. 104:16868-16873.

16. Rickgauer J. P., Fuller D.N., Grimes S., Jardine P.J., Anderson D., Smith D. E. (2008) Portal motor velocity and internal force resisting viral DNA packaging in bacteriophage phi29. Biophys. J. 94:159-167.

17. Tsay J.M., Sippy J., Feiss M. & Smith D.E. (2009) The Q motif of a viral packaging motor governs its force generation and communicates ATP recognition to DNA interaction. Proc. Natl. Acad. Sci. U. S. A. 106:14355-14360.

18. Moffitt J.R., Chemla Y.R., Aathavan K., Grimes S., Jardine P.J., Anderson D.L., Bustamante C. (2009) Intersubunit coordination in a homomeric ring ATPase. Nature. 457:446-450.

19. Tsay J. M., Sippy J., DelToro D., Andrews B.T., Draper B., Rao V., Catalano C.E., Feiss M., Smith D.E. (2010) Mutations altering a structurally conserved loop-helix-loop region of a viral packaging motor change DNA translocation velocity and processivity. J. Biol. Chem. 285:24282-24289.

20. Chistol G., Liu S., Hetherington C.L., Moffitt J.R., Grimes S., Jardine P.J., Bustamante C. (2012) High degree of coordination and division of labor among subunits in a homomeric ring ATPase. Cell. 151:1017-1028.

21. Kottadiel V.I., V.B. Rao and Y.R. Chemla (2012). The dynamic pause-unpackaging state, an off-translocation recovery state of a DNA packaging motor from bacteriophage T4. Proc Natl Acad Sci U S A. 109:20000-20005.

22. Migliori A.D., Keller N., Alam T.I., Mahalingam M., Rao V.B., Arya G., Smith D.E. (2014) Evidence for an electrostatic mechanism of force generation by the bacteriophage T4 DNA packaging motor. Nature Communications. 5:4173.

23. Berndsen Z.T., N. Keller, Grimes S., Jardine P.J., Smith D.E. (2014) Nonequilibrium dynamics and ultraslow relaxation of confined DNA during viral packaging. Proc Natl Acad Sci USA. 111:8345–8350.

24. Morais M.C., Koti J.S., Bowman V.D., Reyes-Aldrete E., Anderson D.L., Rossmann M.G. (2008) Defining molecular and domain boundaries in the bacteriophage phi29 DNA packaging motor. Structure. 16:1267-1274.

25. Tang J, Olson N., Jardine P.J., Grimes S., Anderson D.L., Baker T.S. (2008) DNA poised for release in bacteriophage ø29. Structure. 16:935-943.

26. Liu S., Chistol G., Hetherington C.L., Tafoya S., Aathavan K., Schnitzbauer J., Grimes S., Jardine P.J., Bustamante C. (2014) A viral packaging motor varies its DNA rotation and step size to preserve subunit coordination as the capsid fills. Cell. 157:702-713.

27. Fuller D.N., Gemmen G.J., Rickgauer J.P., Dupont A., Millin R., Recouvreux P., and Smith D.E. (2006) A general method for manipulating DNA sequences from any organism with optical tweezers. Nucleic Acids Res. 34:e15.

28. Rickgauer J. P., Fuller D.N. and Smith D.E. (2006) DNA as a metrology standard for length and force measurements with optical tweezers. Biophys. J. 91:4253-4257.

29. DelToro D. and Smith D.E. (2014) Accurate measurement of force and displacement with optical tweezers using DNA molecules as metrology standards. Appl Phys Lett. 104:143701.

30. Wang M.D., Schnitzer M.J., Yin H., Landick R., Gelles J., Block S.M. (1998) Force and velocity measured for single molecules of RNA polymerase. Science. 282:902-907.

31. Keller D. and Bustamante C. (2000) The mechanochemistry of molecular motors. Biophys. J. 78:541-556.

32. Keller N., Grimes S., Jardine P.J., Smith D.E. (2014) Repulsive DNA-DNA interactions accelerate viral DNA packaging in phage phi29. Phys. Rev. Lett. 112:248101.

33. Tao Y., Olson N.H., Xu W., Anderson D.L., Rossmann M.G., Baker T.S. (1998) Assembly of a tailed bacterial virus and its genome release studied in three dimensions. Cell. 95:431-437.

34. Xiang Y., Morais M.C., Battisti A.J., Grimes S., Jardine P.J., Anderson D.L., Rossmann M.G. (2006) Structural changes of bacteriophage phi29 upon DNA packaging and release. EMBO J. 25:5229-5239.

35. Fokine A., Chipman P.R., Leiman P.G., Mesyanzhinov V.V., Rao V.B., Rossmann M.G. (2004) Molecular architecture of the prolate head of bacteriophage T4. Proc. Natl. Acad. Sci. U. S. A. 101:6003-6008.

36. Jiang W., Chang J., Jakana J., Weigele P., King J W. Chiu (2006) Structure of epsilon15 bacteriophage reveals genome organization and DNA packaging/injection apparatus. Nature. 439:612-616.

37. Lander G.C., Tang L., Casjens S.R., Gilcrease E.B., Prevelige P., Poliakov A., Potter C.S., Carragher B., Johnson J.E. (2006) The structure of an infectious P22 virion shows the signal for headful DNA packaging. Science. 312:1791-1795.

38. Tang J., Lander G.C., Olia A.S., Li R., Casjens S., Prevelige P. Jr, Cingolani G., Baker T.S., Johnson J.E. (2011) Peering down the barrel of a bacteriophage portal: The genome packaging and release valve in p22. Structure. 19:496-502.

39. Olia A. S., P.E. Prevelige Jr, ..., G. Cingolani 2011. Three-dimensional structure of a viral genome-delivery portal vertex. Nat. Struct. Mol. Biol. 18:597-603.

40. Casjens S., Wyckoff E., Hayden M., Sampson L., Eppler K., Randall S., Moreno E.T., Serwer P. (1992) Bacteriophage P22 portal protein is part of the gauge that regulates packing density of intravirion DNA. J. Mol. Biol. 224:1055-1074.

41. Petrov A.S., Lim-Hing K. and Harvey S.C. (2007) Packaging of DNA by bacteriophage Epsilon15: Structure, forces, and thermodynamics. Structure. 15:807-812.

42. Kindt J., Tzlil S., Ben-Shaul A. & Gelbart W.M. (2001) DNA packaging and ejection forces in bacteriophage. Proc. Natl. Acad. Sci. U. S. A. 98:13671-13674.

43. Purohit P.K., Kondev J. and Phillips R. (2003) Mechanics of DNA packaging in viruses. Proc. Natl. Acad. Sci. U. S. A. 100:3173-3178.

44. Petrov A.S. and Harvey S.C. (2007) Structural and thermodynamic principles of viral packaging. Structure. 15:21-27.

45. Evilevitch A., Castelnovo M., Knobler C.M., Gelbart W.M. (2004) Measuring the force ejecting DNA from phage. J Phys Chem B. 108:6838-6843.

46. De Frutos M., Leforestier A. and Livolant F. (2014) Relationship between the genome packaging in the bacteriophage capsid and the kinetics of DNA ejection. Biophys Rev Lett. 9:81-104.

47. Qiu X., Rau D.C., Parsegian V.A., Fang L.T., Knobler C.M., Gelbart W.M. (2011) Salt-dependent DNA-DNA spacings in intact bacteriophage λ reflect relative importance of DNA self-repulsion and bending energies. Phys. Rev. Lett. 106:028102.

48. Lander G.C., Johnson J.E., Rau D.C., Potter C.S., Carragher B., Evilevitch A. (2013) DNA bending-induced phase transition of encapsidated genome in phage λ. Nucleic Acids Res. 41:4518-4524.

49. Moffitt J.R., Chemla Y.R., Aathavan K., Grimes S., Jardine P.J., Anderson D.L., Bustamante C. (2009) Intersubunit coordination in a homomeric ring ATPase. Nature 457, 446–450

50. Yu J., Moffitt J., Hetherington C., Bustamante C., Oster G. (2010) Mechanochemistry of a viral DNA packaging motor. J. Mol. Biol. 400, 186–203

51. Xing J., Wang H., Oster G. (2005) From continuum Fokker-Planck models to discrete kinetic models. Biophys. J. 89:1551–63

52. Voter A. (2007) Introduction to the kinetic Monte Carlo method. Radiation Effects in Solids, 1–23.

Chapter IV

Future Directions and Final Thoughts

A. Future Directions

The results presented in Chapters II and III show that viral DNA packaging is more complex and rich in interesting physical phenomena than previously thought. These findings, combined with related experimental and theoretical findings by other groups, directly motivate a number of follow up experiments. Before discussing specific experimental details, I present an overview of our current understanding of viral DNA packaging and the various parameters that have been shown to or are hypothesized to directly influence the dynamics of the reaction. Then I will discuss in more detail one particular set of experiments I am currently in the process of running and can show promising preliminary data for. The flow chart in Fig. 4.2 demonstrates the relationship between various control parameters, experimental observables, and the underlying physical phenomena that give rise to these observables and will serve as a roadmap for experimental design. For example, we now know that DNA is not in quasistatic equilibrium and that this leads to the experimental observables of motor slowing via pausing and slowed ATP binding, however we have yet to explore the large space of control parameters that we either know or hypothesize will affect these nonequilibrium dynamics. One such parameter is DNA packaging rate. It is likely that the rate at which DNA is packaged into the prohead has a significant influence on the formation of nonequilibrium structures so it would be of interest to run similar experiments as those described in this work while controlling the packaging rate with either temperature or changes to the [nucleotide]s. Temperature itself is also a controllable parameter that has

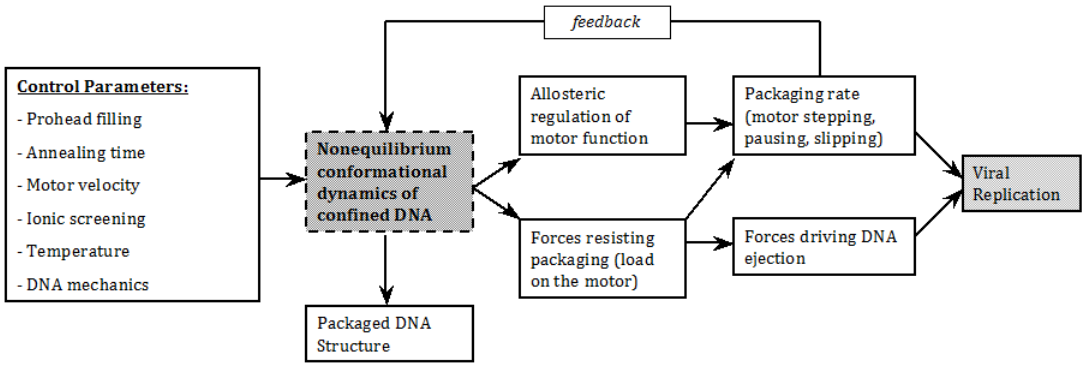

Figure 4.1. Flow chart illustrating our understanding of the underlying biophysical phenomena involved in DNA packaging. The left most box lists what we believe are the most important parameters likely to have significant effects on the nonequilibrium dynamics of the DNA. The experiments presented in chapter II begin to address some of these such as prohead filling and annealing time, however each of those has the potential to be explored in much greater depth. Our lab has also already performed systematic studies of motor velocity under different ionic screening conditions; however, in light of our new understanding it could be beneficial to repeat/expand upon what has already been done. On the right side of the flow chart are listed the various experimental observables and the underlying processes that control them. For instance, we now know that the motor velocity is a complex combination of several different effects. This work established protocols for observing these phenomena. For instance, the average residence time of γS-ATP docked to the motor is a simple and information rich piece of data that can be collected under all experimentally interesting conditions to assess the extent of allosteric slowing that has taken place when dwell time distributions cannot be collected.

been shown to significantly influence the energetics of DNA ejection (1,2), so it is very likely that it will also affect the nature of the nonequilibrium dynamics during packaging. The flow chart in Fig 4.2 also makes it clear that new experimental techniques besides our single-molecule packaging assays will be necessary to fully address the questions at hand. For instance, Cryo-electron microscopy is a powerful tool that allows for the direct observation of DNA structure and has been utilized extensively by other groups as well as by our own to study packaged DNA. However, in light of our recent findings, several new experiments can be devised that would provide much needed structural information of the DNA structure. For example, one could initiate packaging in bulk and freeze aliquots of the reaction at different time points both during and after the reaction has completed to assess the extent and timescale of structural rearrangements, given that they are significant enough to observe. It would be particularly interesting to tract the inter-axial spacing's as a function of time after packaging. Also included in the flowchart are DNA ejection forces, which up until now have not been discussed, however the strong connection between the forces measured during packaging and those that drive ejection suggest that nonequilibrium effects may well manifest themselves in the ejection process as well. Indeed, significant pausing has been observed in single-molecule ejection experiments. As I will discuss in more detail below, the measurement of DNA ejection forces is a powerful tool for observing nonequilibrium effects, particularly the long time scale relaxations that are so difficult to measure serially in single molecule experiments.

1. Achieving long timescale aging experiments with DNA ejection

Of all the possible follow up experiments suggested by our recent findings, perhaps the most important will be achieving a more complete understanding of the

timescales involved in the slow relaxation we observed in our single molecule experiments. If a true upper bound can be placed on the relaxation time it would go a long way in helping pinpoint the underlying physics controlling the relaxation dynamics of the tightly confined DNA. This will be important from both a pure physics point of view as well as a biological one, since it is still unknown how these nonequilibrium effects influence the subsequent ejection process that can happen long after packaging has completed. Because technical limitations of our single molecule experiments make accessing very long timescales unfeasible, other experiments must be devised to study these timescales. It should also be noted that the relaxation time of the DNA is expected to continue growing as procapsid filling increases beyond 75%, thus making measurements of DNA relaxation via single molecule experiments even more difficult.

One way we have devised to overcome this limitation is through analysis of DNA ejection forces in bulk using an approach recently developed by Evilevitch, Knobler, Gelbart and coworkers and applied to studies of phage lambda (3). The forces driving DNA ejection are believed to be the same forces that resist packaging so these measurements are complementary to our single molecule packaging measurements and will provide an independent assessment of internal force to which we can compare our more recent estimates from single molecule packaging studies. This method involves triggering DNA ejection while applying an osmotic pressure to partly or wholly inhibit the process. A known osmotic pressure is applied by adding high molecular weight polyethylene glycol (PEG), which is too large to permeate the procapsid and thus creates an osmotic potential difference across the procapsid wall. The ejection force may be deduced by a theoretical analysis that relates force and applied osmotic pressure, however

there are several issues with that conversion procedure and so I will refrain from using it in this discussion. The dependence of ejection force on the length of DNA left inside the procapsid can be determined by varying the PEG concentration. We are currently in the process of adapting these experiments to the phi29 system and have developed an extended protocol for studying nonequilibrium effects and the various factors that influence them. Because the phage particles remain relatively stable after packaging *in vitro*, it is possible to age the particles for up to few days at room temperature prior to triggering ejection, a timescale orders of magnitude longer than we could reach with single molecule relaxation experiments alone. The experiments described in Ref. (4) involve triggering ejection from phage lambda *in vitro* by addition of recombinant LamB protein, the native cell surface ligand that triggers ejection from mature phage. The cell surface ligand for phi29 is not known so we are exploring alternate means of triggering ejection. The ejection experiments in Ref. (4) utilized mature phage particle (mature phage has the tail through which ejection occurs natively) purified from the native cellular substrate, however, because the cell surface ligand for phi29 is not known, we have decided to just extend our already well established *in vitro* packaging assay (3) into an ejection assay. The protocol involves combining recombinant gp-16, pRNA, purified empty procapsids, and gp3-DNA in the presence of ATP to initiate packaging. ~10 min later DNAse is added to digest unpackaged DNA and the reactions are combined with the appropriate amount of 50% PEG 8000 (w/v), mixed very thoroughly, and placed at 50°C for 30 min to trigger ejection. Finally, proteinase K is added to digest gp-3 and procapsid protein to release un-ejected DNA.

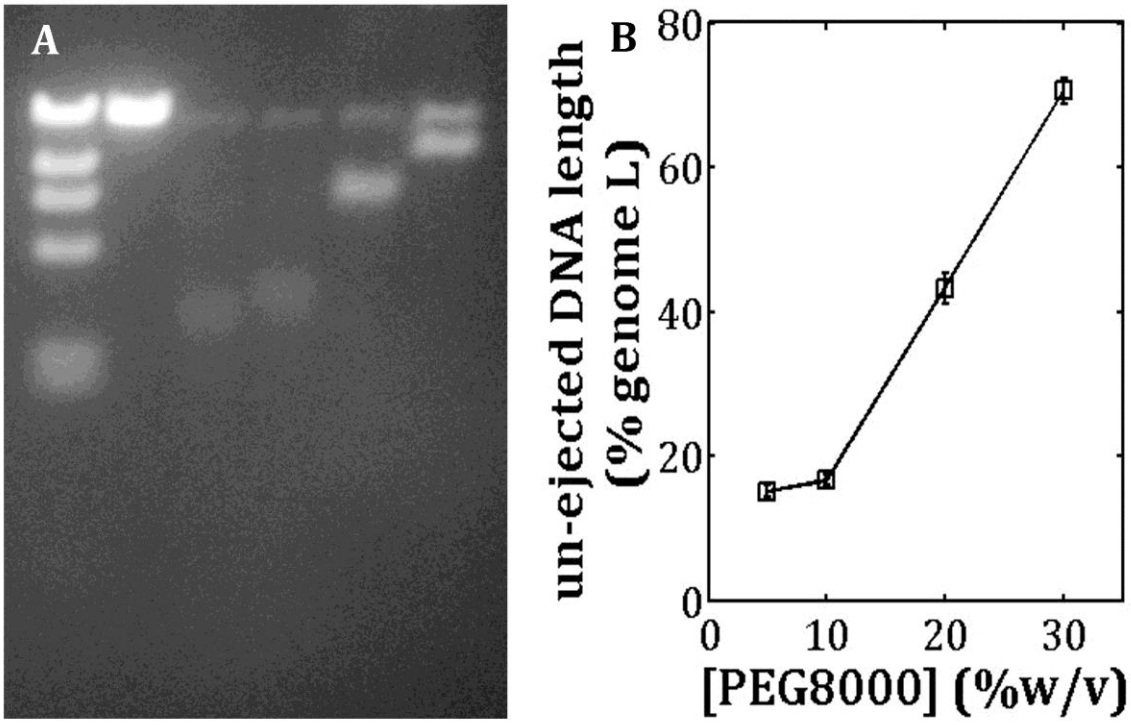

Figure 4.2. Osmotic suppression of ejection. (A) Lane 1, λ HindIII ladder; lane2, 500ng protease digested gp3-DNA; lane 3, ejection with 5% PEG (w/v); lane 4, ejection with 10% PEG (w/v); lane 5, ejection 20%PEG (w/v); lane 6, ejection 30%PEG (w/v). The top band in all experimental lanes is full length un-ejected full length phi29 DNA. Ejection was carried out in our standard packaging buffer and triggered at 50ºC within 30 min of initiating packaging *in vitro*. **(B)** Average unejected DNA length ± SEM as a function of [PEG] for 3 independent measurements. It should be noted that the buffer conditions do not match those used in Ref. (4) in which the Mg2+ concentration was several fold higher. Ejection can be triggered in high Mg2+ buffers and the average unejected fragment lengths increase as would be expected for conditoins with higher charge screening (data not shown)

SDS is added with loading buffer and the entire mixture is run on a gel. An example gel can be seen in Fig. 4.2A showing ejection into four different PEG concentrations. Fig. 4.2B shows the average un-ejected fragment length of three such experiments. It should be noted that the conversion of these values into osmotic pressures and subsequently into forces is difficult and actually relies on assuming the DNA is perfectly spooled and hexogonally packed, however, regardless of the absolute magnitude of the force, though it would be ideal to know, is not necessary for the purpose of examining parameters that change the ejection force so long as clear differences can be observed that should be sufficient. As in Ref. (4) we are able to control all the solution conditions prior to ejection, however with our system we also achieve much stricter control over the timing between packaging and ejection as well as gain additional control over the packaging conditions. In our assay ejection is assumed to occur through the portal complex after the heat causes the motor to spontaneously dissociate. Preliminary experiments performed in the lab of our collaborators Paul Jardine and Shelly Grimes found that ejection could be triggered by the addition of RNAse and at elevated temperatures. The RNAse degrades the packaging RNA (pRNA) and is thought to help dissociate the motor from the procapsid, however elevated temperatures are still necessary. In more recent experiments I found that RNAse digestion actually helps very little and the elevated temperature is the primary cause of ejection. Thus I have chosen not use RNAse and just trigger ejection with elevated temperatures only. This has obvious disadvantages but several key advantages that I believe make it the best assay for the problems we wish to address. My biggest concern is that the elevated temperature

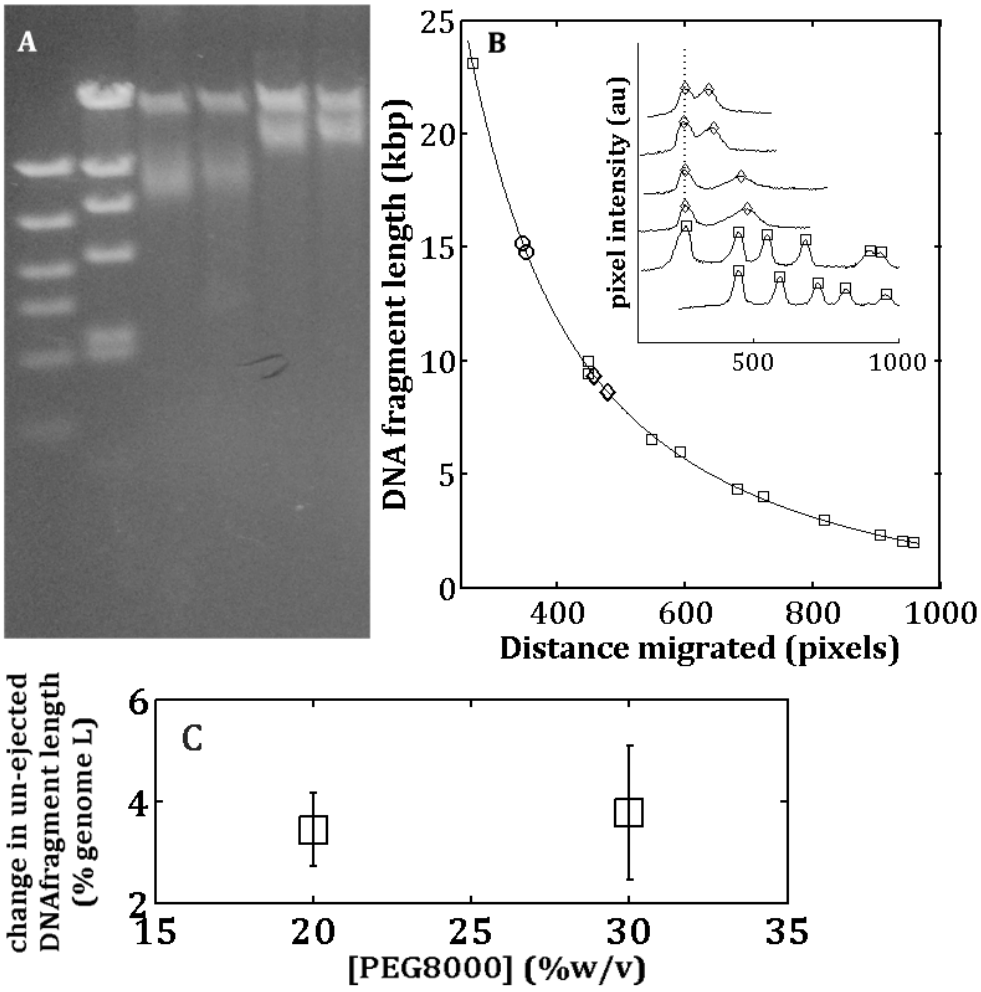

Figure 4.3. DNA ejection after 24hr aging. (A) Lane 1; High DNA Mass ladder (Invitrogen); lane 2, λ HindIII ladder (NEB); lane3, ejection with 20% PEG (w/v) triggered <30 min after initiating packaging; lane 4, ejection with 20% PEG (w/v) after particles were aged for 24hrs; lane 5 and 6 are in 30% PEG, same conditions as lanes 3 and 4. All ejections were carried out at 50ºC in standard packaging buffer. **(B)** Automated fragment length determination. Peaks in the average horizontal pixel intensity from DNA ladder lanes (boxes) are located and used for calibration (fit to the curve). Peaks for ejected DNA at 20 and 30% PEG are plotted as diamonds and circles respectively. Inset shows raw pixel intensity plots for each lane. Dashed line are the un-ejected DNA bands that serve as an internal control. Only gels where the un-ejected DNA in each experimental lane run in parallel (as judged by eye) are kept for analysis. Image processing and analysis was done with a custom Matlab script. **(C)** Average ± SEM of 3 independent measurements of the change in the un-ejected fragment length after 24 hr aging at RT.

may “erase” some of the nonequilibrium structure formed during packaging and I have yet to fully address this concern. Another concern is that the [PEG] to osmotic pressure relationship is temperature dependent and will have to be taken into account prior to calculating pressure and subsequently force. Nonetheless, preliminary experiments indicate that the fraction of DNA ejected in the presence of 20 and 30% PEG (w/v) is significantly reduced, by 3.4 ± 0.7% (of the genome length) and 3.8 ± 1.3% respectively, after aging the particles for 24 hours from the time packaging was initiated (mean ± SEM for three independent measurements). An example of one such experiment is shown in Fig. 4.3A. Fig. 4.3B illustrates the method with which I calculate precise DNA fragment lengths for each separate gel. Briefly, average horizontal pixel intensities are calculated for each lane and peaks in these plots are identified. These points are then used as a gel/experiment specific calibration and unknown fragment lengths are calculated from the fitted model. The error associated with each individual measurement can be calculated using internal lane controls however this analysis has yet to be performed. Previous studies of ejection forces from phage lambda and HSV-1 did not take into account the time between the packaging reaction and ejection nor did they report these times, therefore it is unknown how their results are affected (4). In addition to aging the particles it is possible to control the packaging rate with both [nucleotide] and temperature in order to determine the extent to which packaging rate contributes to the formation of nonequilibrium structures. I favor controlling the packaging rate thorough controlling nucleotide concentrations because temperature also influences the relaxation dynamics of the DNA independent of its influence on packaging rate. Preliminary results

indicate both depressed temperatures (10°C) and low [ATP] cause significant shifts in ejected fragment length (data not shown).

B. Concluding Remarks

Prior to initiating the work presented in this dissertation, two major assumptions in the field remained unvalidated. The first assumption was that viral DNA packaging is a quasistatic thermodynamic process, or in other words, that the packaged DNA molecule can rapidly relax to its energetically minimized structure inside the viral procapsid at all points during the packaging reaction. This assumption has been fundamental to construction of most theoretical models of viral DNA packaging (5-7). The second assumption was fundamental to the methods with which we inferred forces resisting DNA packaging from measurements of motor velocity in single molecule experiments. The assumption was that the observed slowing of the motor with procapsid filling was entirely due to forces resisting DNA confinement that load the motor. Because the force-velocity relationship can be reliably measured this assumption allowed the velocity-filling relationship to be re-interpreted as a force-filling relationship, a critical step in our previous analysis protocol (8-10). One of the major problems with these assumptions remaining unvalidated was that significant discrepancies between theoretical predictions and experimental measurements of the forces resisting packaging existed which could not be properly resolved until the validity of these assumptions had been checked. The most fundamental act of the scientific process is the comparison of theoretical predictions with experimental data. Inconsistencies in this relationship drive the creation of new theories

and highlight the need for new experiments. The work presented in this dissertation is a first attempt at addressing the validity of these two assumptions and is thus of principal importance to progress in the field.

Beyond immediate impact to the field of viral genome packaging, the work presented in in Chapter II makes important contributions to more general problems in soft-matter physics. The fundamental physics governing the dynamics of polymers under various confinement geometries has been attracting a great deal of scientific attention lately with most experimental studies utilizing DNA as the model polymer and exploring 1 and 2-D confinement over a range of conditions (11-14). The case of 3-D confinement, particularly tight 3-D confinement, had yet to be explored experimentally. This is in large part due to obvious technical difficulties associated with fabricating nanoscale compartments, controllably inserting biological or synthetic polymers into these structures, and finding a means with which to measure their dynamics in these containers. DNA packaging in bacteriophage is a remarkable realization of this phenomenon in a naturally occurring system and our stall-restart experiments represent the first attempts to successfully probe polymer dynamics in the regime of tight 3-D confinement. We find striking features emerge in this regime; for instance, we measure DNA relaxation at ~75-80% prohead filling and show that the system exhibits ultra-slow relaxation dynamics, a feature not observed for the cases of tight 1 and 2-D confinement (12,13) and not observed at lower prohead fillings. One interpretation of this finding is that, once both the length of the DNA molecule and its volume fraction inside the viral procapsid increase past a certain point, molecular crowding makes large scale structural rearrangements increasingly difficult and the DNA undergoes a transition of some type into a phase

exhibiting glassy dynamics. It is not possible to determine from our experiments whether this transition is in fact the classical polymer glass transition however it is tempting to speculate that the DNA is in-fact undergoing a type of filling induced glass or "jamming" transition similar to what is observed in various granular systems at high packing densities. In a sense, one could say the system starts exhibiting glassy dynamics at the point when the ratio of the relaxation time of the DNA and the measurement time, $\tau_{relaxation}/\ \tau_{measurement,}$ exceeds unity. From the perspective of the motor, $\tau_{measurement} = \tau_{dwell}$, since it is at this point that the DNA is no longer in quasistatic equilibrium with respect to the perturbations produced by the packaging motor (ie. stepping). At ~75% procapsid filling we find that the lower bound of 10 min placed on the relaxation time by our experiments well exceeds the time normally taken to package the entire genome. Such glassy dynamics have been found to occur in other biological systems were long biopolymers are packed at similarly high densities. For instance, ultra-slow relaxation was shown to play a major role in maintaining the specific 3-dimensional architecture of the eukaryotic chromosomes (15) within the nucleus and recent theoretical studies predict that glassy dynamics should occur in any polymeric system in which the volume fraction of polymer molecule exceeds 0.4, regardless of the geometry of the container (16). The volume fraction within many phages is believed to reach this critical value. Recently published Isothermal-titration-calorimetry data on the energetics of DNA ejection from Herpes virus (HSV-1) found striking evidence for the occurrence of a solid- to-fluid like phase transition when the temperature of the reaction was raised to roughly the internal body temperature (1). The fact that such a transition is observed to occur at temperatures higher but still relatively close to the temperature we conduct our packaging experiments

at lends support to the hypothesis that an opposite transition, from a fluid-like to solid-like phases, must at some point also occur as packing densities increase. Indeed, DNA is well known to transitions through various liquid crystalline phases as the concentrations begin reaching those within the viral procapsid at even low to intermediate fillings (17).

Although the change in force implied by the motor acceleration after long stalls is not large enough to account for the entire magnitude of the difference between theoretical and experimental estimates of the force resisting packaging, our results still represent strong evidence against the quasistatic assumption and highlight the need to take nonequilibrium effects into account when developing more realistic theories of DNA packaging and ejection forces. From a more philosophical perspective, the work presented in Chapter II provides a clear illustration of how common biological processes can exist far from equilibrium and how their study can provide a unique testing ground for the underlying physics. We hope that the work presented here serves as a starting point for the development of new theories of polymer dynamics under strong confinement and helps continue to draw attention the importance such nonequilibrium polymer effects in biological processes.

In addition to building a strong case against the validity of the quasistatic assumption, in Chapter III we presented strong evidence against the validity of the other fundamental assumption I mentioned at the start of the chapter; that force and procapsid filling have the same effect on the motor. In fact, we found that this faulty assumption was the primary source of the discrepancy between theoretical predictions of the forces resisting DNA packaging and the forces previously estimated from our single molecule experiments. Although this finding complicated the interpretation of the results presented

in Chapter II, I find that the two data sets complement each other nicely, and when viewed as a whole provide a much clearer picture of the dynamic relationship between the packaging motor and the DNA. It is now clear that when studying the DNA dynamics one cannot ignore specifics of the packaging motor kinetics and when studying the packaging motor kinetics one cannot ignore the influence of the packaged DNA dynamics. This relationship is depicted as the feedback look in Fig. 4.1. So can we say yet what the ultimate "purpose" for the allosteric control mechanism is? Well, although such a velocity control mechanism may be necessary to trigger termination during headful packaging in phages such as lambda and it is tempting to speculate that the mechanism we observe is in fact of the same origin, I find this to be an unlikely hypothesis given that phi29 packages a linear genome and does not need to cleave its packaging substrate at a specific location. Given the timescales likely involved in the splitting of the two classes of phage it would seem unlikely that such a mechanism would have persisted for so long without a clear fitness advantage. Therefore, I favor a scenario in which the allosteric regulation mechanism evolved for the purpose of minimizing DNA jamming and the formation of highly nonequilibrium structures within the procapsid, as we have shown these can stall the motor and prevent packaging from going to completion. That motor pausing is reduced after long stalls and is highly heterogeneous from one particle to the next provides strong evidence that pauses occur in response to nonequilibrium DNA dynamics, leading one to suspect that the reduced ATP binding rate has a similar purpose. There is still a great deal of mystery as to the exact mechanism by which the motor complex and packaged DNA engage in such long distance allosteric communication, and in fact there is as of yet no crystal structure of gp-

16 with which one could make educated guesses about the communication pathway. Structural studies, possibly asymmetric Cryo-EM reconstructions focusing specifically on the motor complex captured in various stages of packaging could go a long way in helping to construct a plausible mechanism for this phenomenon. In addition, expanded single molecule analysis, particularly high resolution measurements with various mutant motor complexes could potentially provide important insight into this problem. I believe such studies are already underway in the lab of our collaborators. Finally, it would be very interesting to know if a similar control mechanism exists in other phage systems, particularly those that package by a headful mechanism such as lambda. Our lab also studies lambda phage and we are in a unique position to test this. Because lambda's genome is so much longer than phi29's, tracking packaging to high filling is much more difficult, however the allosteric mechanism at work in phi29 appears to be extremely sensitive to packaged DNA structure and signs of this regulatory mechanism are visible as early as 10-20 % filling so perhaps similar behavior is responsible for the changes in velocity observed at earlier stages of packaging in lambda as well. I think the best place to start would be tracking γS-ATP residence times as a function of prohead filling as we did in Chapter III. The long timescales of γS-ATP induced pauses and their sensitive dependence on filling make this a relatively easy yet potentially information rich experiment, assuming the lambda terminase complex packages by a similar mechanochemical mechanism as phi29.

The final picture that emerges from the findings presented in this dissertation is that viral DNA packaging is more complex and rich in interesting physical phenomena than previously thought. It is now clear that the high density packaging of DNA by phage

phi29 is achieved only through sophisticated interactions between of the packaged DNA and the packaging motor complex in which the reaction rate is allosterically tuned by the DNA density and conformation via a complex feedback control mechanism. In turn the packaging rate influences the DNA conformation such that at high filling we see packaging proceed in a highly heterogeneous manner as the motor adjusts its ATP binding rate and frequently enters into paused states, likely allowing nonequilibrium DNA conformations to partially relax so that packaging can continue without stalling permanently.

C. References

1. Sae-Ueng U., Li D., Zuo X., Huffman J.B., Homa F.L., Rau D. & Evilevitch A. (2014) Solid-to-fluid DNA transition inside HSV-1 capsid close to the temperature of infection. Nature Chemical Biology 10, 861–867

2. Liu T., Sae-Ueng U., Lia D., Lander G.C., Zuoc X., Jönsson B., Rau D., Shefer I., and Evilevitch A. (2014) Solid-to-fluid–like DNA transition in viruses facilitates infection. Proceedings of the National Academy of Sciences U. S. A., 111, pp. 14675–14680

3. Guo P., Grimes S. & Anderson D. (1986) A defined system for in vitro packaging of DNA-gp3 of the Bacillus subtilis bacteriophage phi29. Proc. Natl Acad. Sci. USA 83, 3505–3509

4. Evilevitch A., Lavelle L., Knobler C.M., Raspaud E. & Gelbart W.M. (2003) Osmotic pressure inhibition of DNA ejection from phage. Proc Natl Acad Sci U S A 100(16): 9292-9295.

5. Kindt J., Tzlil S., Ben-Shaul A. & Gelbart W.M. (2001) DNA packaging and ejection forces in bacteriophage. Proc Natl Acad Sci U S A 98(24): 13671-13674.

6. Tzlil S., Kindt J.T., Gelbart W.M. & Ben-Shaul A. (2003) Forces and pressures in DNA packaging and release from viral capsids. Biophys J 84(3): 1616-1627.

7. Purohit P.K., Kondev J. & Phillips R. (2003) Mechanics of DNA packaging in viruses. Proc Natl Acad Sci U S A 100(6): 3173-3178.

8. Smith D.E., Tans S.J., Smith S.B., Grimes S., Anderson D. L. & Bustamante C. (2001) The bacteriophage phi29 portal motor can package DNA against a large internal force. Nature 413(6857): 748-752.

9. Rickgauer, J. P., Fuller D.N., Grimes S., Jardine P.J., Anderson D., Smith D. E. (2008) Portal motor velocity and internal force resisting viral DNA packaging in bacteriophage phi29. Biophys J 94(1): 159-167.

10. Fuller D.N, Rickgauer J.P., Grimes S., Jardine P.J., Anderson D., Smith D. E (2007) Ionic effects on viral DNA packaging and portal motor function in bacteriophage phi 29. Proc Natl Acad Sci U S A 104(27): 11245-11250.

11. Sakaue T. (2007) Semiflexible polymer confined in closed spaces. Macromolecules 40(14): 5206-5211.

12. Reisner W., Pedersen J.N. & Austin R.H. (2012) DNA confinement in nanochannels: Physics and biological applications. Rep Prog Phys 75(10): 106601.

13. Reisner W., Morton K.J., Riehn R., Wang Y.M., Yu Z., Rosen M., Sturm J.C., Chou S.Y., Frey E., Austin R.H. (2005) Statics and dynamics of single DNA molecules confined in nanochannels. Phys Rev Lett 94(19): 196101.

14. Tang J., Levy S. L., Trahan D. W., Jones J.J., Craighead H.G. and Doyle P.S. (2010) Revisiting the conformation and dynamics of DNA in slitlike confinement. Macromolecules 43(17): 7368-7377.

15. Lieberman-Aiden E., van Berkum N.L., Williams L., Imakaev M., Ragoczy T., Telling A., Amit I., Lajoie B.R., Sabo P.J., Dorschner M.O., Sandstrom R., Bernstein B., Bender M.A., Groudine M., Gnirke A., Stamatoyannopoulos J., Mirny L.A., Lander E.S., and Dekker J. (2009) Comprehensive mapping of long range interactions reveals folding principles of the human genome. Science 326(5950): 289–293. doi:10.1126/science.1181369

16. Kang H., Yoon Y., Thirumalai D., Hyeon C. (2015) Glassy dynamics distinguishes chromosome organization across organisms. arXiv:1506.01089 [cond-mat.soft]

17. Livolant F. (1991) Ordered phases of DNA in vivo and in vitro. Physica A: Statistical Mechanics and its Applications, 176 (1), pp. 117-137